7-1-1991

Bremsstrahlung and Energetic Electrons in Supernovae

Donald D. Clayton
Clemson University, claydonald@gmail.com

Lih-Sin The
Clemson University

THE ASTROPHYSICAL JOURNAL, 375:221–238, 1991 July 1

BREMSSTRAHLUNG AND ENERGETIC ELECTRONS IN SUPERNOVAE

DONALD D. CLAYTON AND LIH-SIN THE
Department of Physics and Astronomy, Clemson University, Clemson, SC 29634-1911
Received 1990 June 26; accepted 1990 December 17

ABSTRACT

We first present explicit Monte Carlo calculations of the rate of Compton scattering and of the spectrum of recoil electrons per gram at discrete depths within models of supernovae. The abundant fast recoil electrons produce many interesting secondary physical processes, foremost of which are bremsstrahlung and X-ray lines created during collisions with ions as those electrons slow down. Our major objective is to calculate the bremsstrahlung emissivity within supernova interiors. Such bremsstrahlung power must exist in all supernovae that are bolometrically powered by radioactive decay; it requires no collisional shocks between fluid elements for its creation. The total power in bremstrahlung production is typically 1×10^{-3} of the total radioactive power emitted as ^{56}Co and ^{57}Co gamma rays that initiate these processes. We calculate the spectrum of the bremsstrahlung emissivity and show it to be $E^{-1.3}$ for a wide range of supernova models. We also calculate the radial and temporal dependence of that emissivity for two models of SN 1987A and for one model of a Type Ia and of a He core explosion model of a Type Ib. The spectrum emerging from the surface (the luminosity), which we then evaluate by Monte Carlo techniques, is sensitive to the photoelectric opacity and is inverted by it—roughly $F(v) \propto v^{1.0-1.5}$; i.e., the spectral luminosity of the bremsstrahlung component increases slowly between 1 and 30 keV even though the emissivity declines with energy within that energy band. We find the bremsstrahlung luminosity to dominate that of the primary scattered gammas for $E < 20$ keV. Both X-ray observations of supernovae and of circumstellar matter must take the bremsstrahlung luminosity into account.

Subject headings: gamma rays: general — radiation mechanisms — stars: individual (SN 1987A) — X-rays: sources

1. INTRODUCTION

The prediction that gamma-ray lines from the decay of newly synthesized ^{56}Ni and ^{56}Co (Clayton, Colgate, & Fishman 1969) and ^{57}Co (Clayton 1974) would be detectable from supernovae has been excitingly confirmed through observations of SN 1987A by the Gamma-Ray Spectrometer aboard the *SMM* satellite (Matz et al. 1988; Leising & Share 1990) and by balloon-borne spectrometers (Sandie et al. 1988; Cook et al. 1988; Mahoney et al. 1988; Rester et al. 1989; Tueller et al. 1990). This success was followed by many calculations of the line and continuum spectra of SN 1987A in hard photons, say, greater than 1 keV in energy, under the simplification that no hard photons (other than atomic X-ray lines) are created within the supernova interior beyond those created during the de-excitation of daughter nuclei following radioactive decay (e.g., The et al. 1990a; Kumagai et al. 1989; Woosley et al. 1989). In this simplification the lines either emerge intact or are Compton downscattered to lower energies, creating the continua (e.g., Figs. 7*a*, 7*b* of The et al. 1990a) at energies lower than each line energy.

In the present work we introduce additional hard photons. They are created in supernova interiors by the bremsstrahlung process and are emitted there while fast recoil electrons (recoiling from Compton scattering events with the primary radioactivity gamma rays) scatter from ions during their deceleration to thermal energies. We demonstrate that this process is important to the total X-ray spectrum. Our interest in this was stimulated initially by the excess 16–28 keV and 6–16 keV radiation from SN 1987A observed from the *Ginga* satellite (Tanaka 1988) and by the inability of radioactive gamma lines to account for the flux in those bands (e.g., The et al. 1990a; Kumagai et al. 1989). Although the bremsstrahlung process that we will present also fails to account for those measurements, it is of high interest as a new physical mechanism for hard radiation from supernova interiors. It has no ad hoc elements, but must be present as surely as the gamma rays are present. Indeed, we will show that bremsstrahlung dominate the continuous spectrum below about 20 keV and not only may be detectable directly but will also be an essential ingredient of the ionization balance of circumsupernova material. In a subsequent paper (The, Bridgman, & Clayton 1991) we evaluate other high-energy consequences of the energetic recoil electrons.

Readers wanting a quick sense of our results may wish to read our conclusions section before deciding how thoroughly they wish to read the following sections.

2. COMPTON-RECOIL SPECTRUM

Although the Klein-Nishina cross section for Compton scattering has its largest value in the forward direction, when weighted by the solid angle the most frequent scatterings per unit angle of MeV range photons are near 30°, but with broad angle and energy widths. The most probable electron energy from the scattering of an 847 keV gamma line from ^{56}Co decays, for example, is about 150 keV, but the total energy spectrum is broad from about 650 keV down to only tens of keV. The recoil electron takes on average a significant fraction of the photon energy. Many scattered gammas scatter again and lose more of their initial energy. The et al. (1990a; see also their references to other treatments) calculated this energy transfer explicitly for models of SN 1987A, defining $f_{\rm scat}$ to be a fraction of the total radioactive power that is imparted to recoil electrons within the entire model. Their Figure 6 shows, for example, that $f_{\rm scat}$ declines slowly from about one-half to

about one-third between days 500 and 1000 of SN 1987A. This scattering power manifests itself initially as energetic electrons. Their secondary processes fuel the bolometric light curve (except for those X-rays and gamma rays from the primary radioactivity) and constitute a large fraction of the total available power. These secondary processes are our topic here and in a subsequent work to follow (The et al. 1991).

We first calculate the spectrum and rate of energetic electron production at each depth within the supernova interior. This must be an inherently numerical and model-dependent procedure, but we will find and emphasize accurate approximations having general utility. The Monte Carlo gamma-ray transport code of The et al. (1990a) is modified for this purpose to record the recoil energy of the target electron in addition to the energy and direction of the scattered gamma ray (which has heretofore been the objective of all such calculations). To illustrate we first display the resulting scattering rate per gram at several different depths for a specific model of SN 1987A, model 10hmm of Pinto & Woosley (1988a, b), which we will use to illustrate many of our results. Figure 1 shows for four depths the number rate (not the energy rate) of Compton electrons at 700 days from our calculated spectrum of hard photons at that depth. The deepest layer shown, $m = 14.0\ M_\odot$ inward from the surface at $t = 700$ days, has the largest scattering rate because the gamma flux increases with depth. The shallowest layer shown, at $m = 3.89\ M_\odot$ from the surface has an optical depth at 20 keV of only $\tau_{20} = 0.29$ due to the very large size and low density of that supernova envelope at $t = 700$ days. The shape of the electron spectrum is seen to be almost independent of depth despite the changes in its intensity. This is a consequence of the nearly constant shape of the gamma spectrum with depth. For the existing spectrum of gammas, the recoil spectra of Figure 1 have the approximate shape between 1 keV $< E <$ 3 MeV, the upper limit of energetic electrons, given by

$$d^3n_e/dM\,dE\,dt = A(dP_{\rm scat}/dM) \times \langle {\rm KE_C}\rangle^{-1}(1 + E/E_0)^{-n}\ {\rm g^{-1}\ s^{-1}\ keV^{-1}}\ , \quad (1)$$

where $\langle {\rm KE_C}\rangle$ is the average value of the recoil energy of a Compton electron and has the value $\langle {\rm KE_C}\rangle = 123$ keV for Figure 1, $dP_{\rm scat}/dM$ is the recoil power per gram locally, and the exponent n has the value 2 for SN 1987A but other values for other objects (see below). This approximate recoil spectrum with $n = 2$ is normalized by the constant $A = \langle {\rm KE_C}\rangle \{E_0^2 \int [x\,dx/(1 + x)^2]\}^{-1}$, with $x = E/E_0$, in such a way that when integrated over mass of the entire model and over energy,

$$\int\int E(d^3n_e/dM\,dE\,dt)dM\,dE = P_{\rm scat} = f_{\rm scat}\,L_{\rm nuc}\ . \quad (2)$$

This is achieved in Figure 1 by an energy-break parameter in the range $E_0 = 16$–21 keV. The success of such a fitting function for different times is shown explicitly in Figure 2, where for improved statistics the total scattering rate *for the entire model* is compared to the mass-integrated form of equation (1),

$$d^2n_e/dE\,dt = AP_{\rm scat}\langle {\rm KE_C}\rangle^{-1}(1 + E/E_0)^{-n}\ {\rm s^{-1}\ keV^{-1}}\ , \quad (3)$$

at the times 175, 350, 700, and 1000 days for model 10hmm of SN 1987A. The best fit values for E_0 are, respectively, 15.8, 18.0, 21.4, and 15.5 keV, each with $n = 2$. Clearly the choice $E_0 = 18$ keV for all times would itself give a rough approximation to the electron spectrum in the absence of detailed calculations for model 10hmm of SN 1987A.

From Figures 1 and 2 we reach our first conclusion, viz., that the recoil-electron spectrum in SN 1987A is almost independent of both depth and time. Comparisons with other objects will be made below, where we will find that both E_0 and the exponent of the energy dependence are different in distinctly different objects. Let it be clear that we used our numerical results for all subsequent calculations, however, and not the fitting function. The average recoil energy is given by the differential cross section average of the Compton kinematics

$${\rm KE_C} = h\nu - h\nu' = h\nu[h\nu(1 - \cos\theta)][mc^2 + h\nu(1 - \cos\theta)]^{-1}\ , \quad (4)$$

where θ is the photon scattering angle. When averaged over the entire model and over the gamma spectrum $h\nu$, we find that $\langle {\rm KE_C}\rangle = 123$ keV for those electrons having $E_k > 1$ keV in the 700 days panel of Figure 2, for example. Averages for all models will be listed in tables to follow and typically lie in the range 90–125 keV. It is not a wide variation as long as $t < 1000$ days and the source is a ^{56}Co–derived spectrum. Another model of SN 1987A to be discussed below yields very similar values for $\langle {\rm KE_C}\rangle$. In both models $\langle {\rm KE_C}\rangle$ increases with time because the number of multiple scatterings, which decrease its value, decreases with time; however, it finally plummets as ^{57}Co becomes more active than ^{56}Co. This transition to ^{57}Co dominance was predicted to be of importance in the first announcement of ^{57}Co gammas (Clayton 1974).

To avoid confusion it is essential that the reader be explicitly aware that when we speak of this *electron spectrum* we speak of the spectrum of *initial* energies, immediately after the scattering events. The actual electron spectrum at a given time would be moderated by the rates at which those recoil electrons lose energy by inelastic collisions, and by introducing those new recoils created by Coulomb scattering of free electrons by the

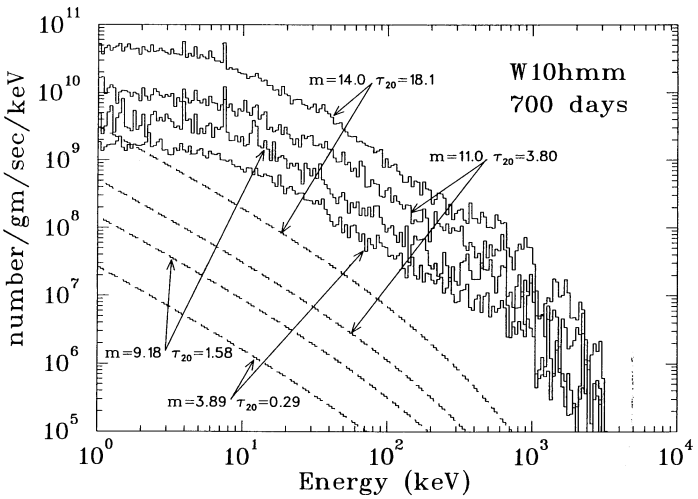

FIG. 1.—Production rate per gram of recoil electrons per keV by Compton scattering of radioactive-decay gamma rays in model 10hmm (Pinto & Woosley 1988a, b) of SN 1987A at day 700. Several separate depths m (in $M_\odot$ from the surface) are indicated in upper histograms (also labeled by 20 keV optical depth τ_{20} to that depth). Steps at 651 keV and 1026 keV are due to backscatter of 847 keV and 1238 keV, respectively. The shape of the electron spectrum is almost depth independent. Smoother lower dashed histograms show the production rate per gram of bremsstrahlung per keV from the same model depths, calculated from the total spectral yield from each electron integrated over its deceleration path according to eq. (4). Bremsstrahlung emissivity spectra are also independent of depth and vary with energy as $E^{-1.3}$.

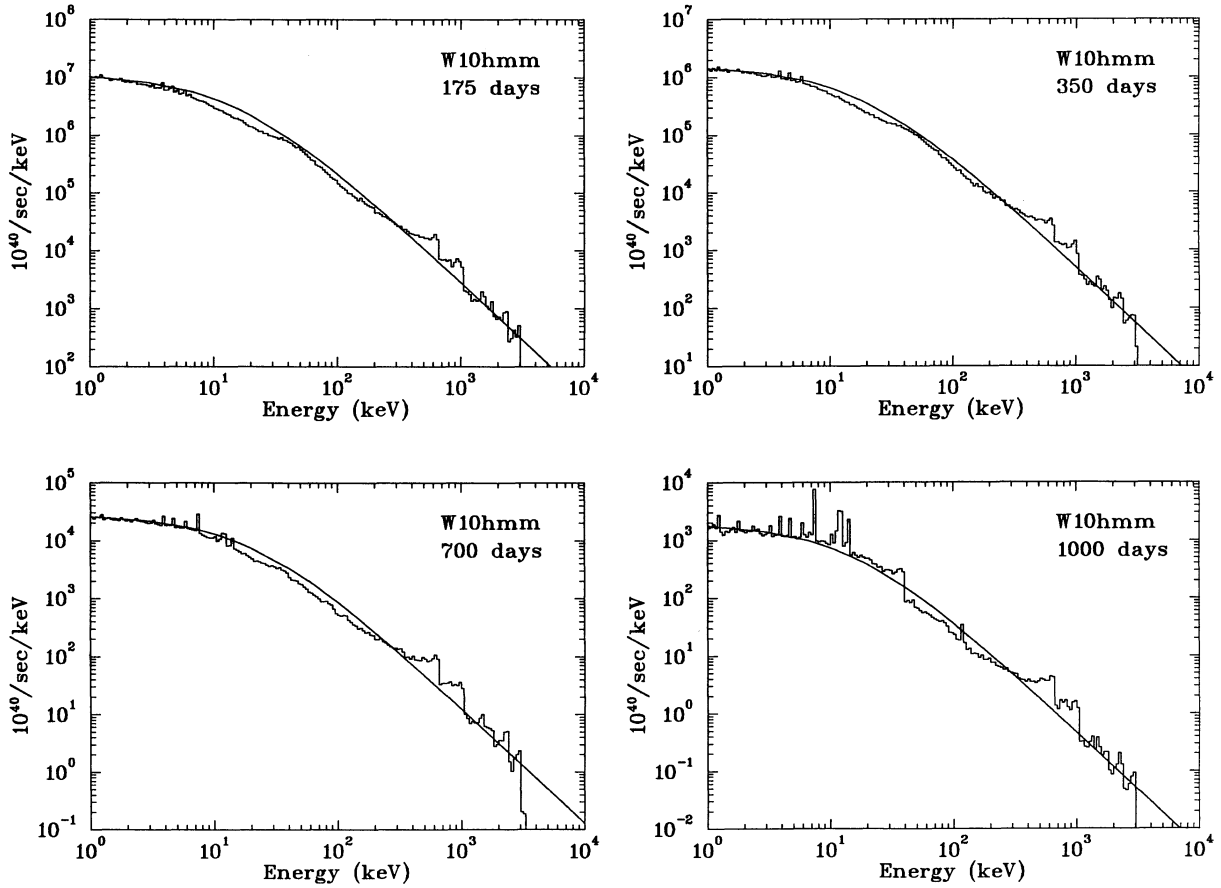

FIG. 2.—Comparisons of the mass-integrated Compton-recoil spectrum for model 10hmm at four distinct times with the approximate fitting function $d^2n_e/dE\,dt = AP_{\rm scat}\langle \mathrm{KE_C}\rangle^{-1}(1 + E/E_0)^{-2}$. Best-fit values of E_0 are 15.5, 18.0, 21.4, and 15.5 keV at t = 175, 350, 700, and 1000 days, respectively. This total spectrum is thereby seen to preserve its shape rather well, whereas Fig. 1 demonstrated it to also be approximately independent of depth. This fitting function is thereby seen to have general utility for model 10hmm; however, our results are in all cases calculated with the actual numerical results of the model, not with the fitting function. Physically different supernova models have similar fitting functions, but with different values for the parameters E_0 and the power-law exponent. Compare with Fig. 11 for a Type Ia model.

Compton electrons, and would also include the thermal spectrum of free electrons. We will not find it necessary to produce such a steady state electron spectrum, because we will prefer to calculate all of the secondary effects produced by each electron during its deceleration, which we will demonstrate to be prompt.

Histogram scatter (at the top of Fig. 1) shows the Monte Carlo statistics attendant to the number of trials—in this case 10^5 radioactive ^{56}Co decays. This portion of our calculations required 16 hr of CPU time on a dedicated Decstation 3100. A particularly interesting feature is the steps at the maximum possible electron energy from a gamma-ray line, which occurs during the 180° scatter of that line. For the 847 keV line, for example, the backscatter loses 651 keV energy to the recoil electron; for the 1238 keV line the maximum energy is 1026 keV. As these recoil electrons slow down, primarily *via* inelastic collisions with atoms and plasma ions, both bremsstrahlung and inner-shell vacancies are created. Both are potentially observable. Another interesting, although not observable, feature of Figures 1 and 2 is the electron-line energies produced by photoelectric absorption of line gammas, e.g., the 7 keV electron line from photoelectric absorption by Fe of the 14 keV gamma line emitted by ^{57}Co.

3. ENERGY-LOSS RATE

The rates of occurrence of specific inelastic events depend upon the numbers of collisions that each recoil electron suffers during its deceleration toward thermal energies. These are dominated by inelastic ionizations of outer-shell electrons, which carry off a mean energy I, whose value is mostly in the 100 eV range for heavy atoms but is smaller for smaller Z. In our numerical example we will take the inelastic collisions to slow the electrons in a gas of atoms of charge Z and atomic weight A according to (Rohrlich & Carlson 1953; ICRU Rept. 37, 1984)

$$dE/dx = 2\pi r_e^2 mc^2 N_{\rm A}\rho(Z/A)/\beta^2 \times [\ln(E_k/I)^2 + \ln(1 + \tau/2) + F^-(\tau) - \delta]\,, \quad (5)$$

where $\tau = E_k/mc^2$ is the electron kinetic energy, I is the mean energy of inelastic excitation and is taken for each element from ICRU Report 37, and the function

$$F^-(\tau) = (1 - \beta^2)[1 + \tau^2/8 - (2\tau + 1)\ln 2]\,.$$

In supernova interiors the factor Z/A is replaced by its mass-weighted average $\Sigma_Z X_Z(Z/A_Z)$. This formula is based on the Møller cross section. In this report we simplify matters a little

by (1) neglecting the small density-correction parameter δ as negligible for this problem; (2) assuming that the electron loses its kinetic energy E_k in a time much shorter than the characteristic evolution time of the remnant, an assumption that we confirm by calculations of the stopping time T_{stop}, as shown for models of various objects to be discussed in Figure 3; and (3) neglecting (for this initial report) electron energy losses due to collisions with free electrons because ionization fractions are sufficiently low ($<10\%$) for $T < 5000$ K that those losses increase dE/dx by less than 20%. It will be clear from equation (8) below, however, that the bremsstrahlung yield depends inversely on the value of dE/dx, so that if plasma processes cause dE/dx to be underestimated by 10%, say, then our bremsstrahlung emissivity will be 10% too high. Because the ionization fraction is such a model-dependent quantity, and indeed one that cannot be calculated without our results, we do not include these plasma losses explicitly in this calculation, which we present by way of a general exposition of bremsstrahlung in supernovae rather than as a model of any particular event. During its deceleration the electron emits bremsstrahlung with roughly 0.3% efficiency (ergs/erg), which we calculate explicitly below, and creates K shell vacancies, which we also calculate but will report in a subsequent publication (The et al. 1991).

For each model we calculate the stopping time and range of characteristic recoil electrons to be sure that it is short compared to the evolution time of the model and to be sure of the approximation that each electron stops at constant density. Figure 3 displays such results for four supernova models used in this paper to illustrate the bremsstrahlung production. The time T_{stop} is defined for initial energy E_k as the time for the electron energy to be degraded from E_k to 1 keV; it is evaluated by $T_{stop} = \int_{E_k}^{1} dE/[v(dE/dx)]^{-1}$. The range is given by $\int_{E_k}^{1} dE/(dE/dx)^{-1}$. Three choices for initial kinetic energy E_k are illustrated in Figure 3: 500 keV (*solid line*), 1 MeV (*dashed line*), and 3 MeV (*dash-dotted line*). The stopping times increase steeply with mass coordinate because the mass density decreases steeply with that coordinate. Except at the very surface, T_{stop} is much smaller than the evolution times of the four models displayed. Although the outermost zone electrons do not stop quickly, their contribution to the bremsstrahlung luminosity was shown by us to be quite small, less than 1%, a result easily understood by confirming that the optical depth $\tau_{10} = 1$ near 10 keV penetrates to much deeper zones than those surface zones. An interesting question that we do not address here is whether fast electrons escape from the models in sufficient numbers to influence other astrophysical questions. The range calculations show, for the models we report,

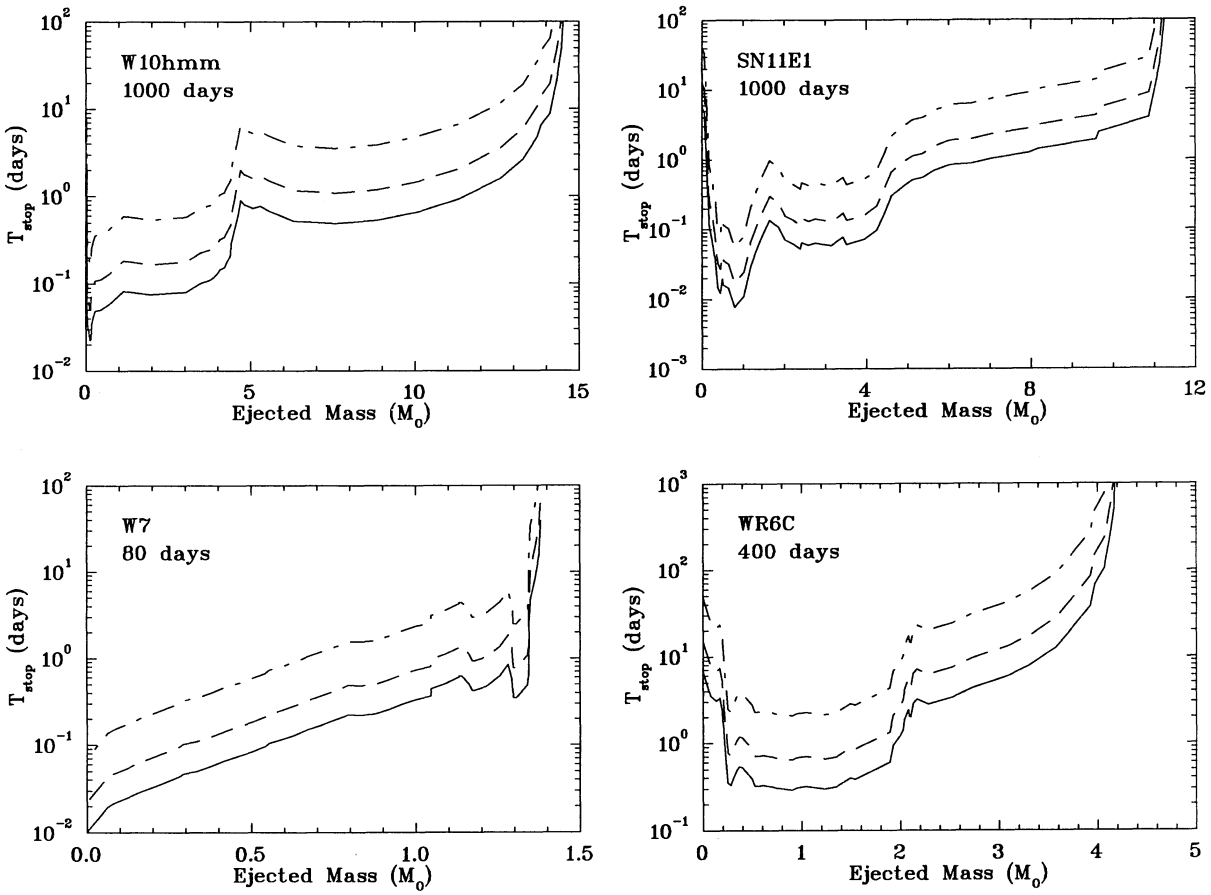

FIG. 3.—Stopping time T_{stop} for recoil electrons in separate mass shells of several supernova models, all of which are discussed in this paper. The three separate curves for each model are for the electron initial energies E_k(initial) = 500 keV (*solid curve*); 1 MeV (*dashed*); 3 MeV (*dash-dotted*). Only in the outermost shells does the stopping time become as long as the time required for such an electron to pass from one zone of the model into a neighboring zone. W10hmm and SN 11E1 are models of SN 1987A, W7 is a model of a Type Ia supernova, and WR6C is a model of a Wolf-Rayet–derived Type Ib model. The stopping time $T_{stop} = \int_{E_k}^{1} dE/[v(dE/dx)]^{-1}$ is for deceleration from E_k to 1 keV. They increase with mass because of the declining density, and the strange structures are the density structures computed for those models by their originators (see text for references).

that the electrons do not migrate to significantly smaller density because of their small motion in mass coordinate. In other words, our approximations are valid for the results we will report.

4. BREMSSTRAHLUNG EMISSIVITY

We take the bremsstrahlung power W at frequency ω for a single electron of velocity v_e in a gas having number density n_Z of element Z, integrated over emission angles, to be given by the sum of the products of the collision rates and the bremsstrahlung emission cross sections:

$$dW/d\omega\, dt = \sum_Z \hbar\omega(d\sigma/d\omega)v_e n_Z\,, \tag{6}$$

where the production cross section for bremsstrahlung is (Jauch & Rohrlich 1976)

$$\omega(d\sigma/d\omega) = (\alpha Z^2 r_e^2 |\,p'\,|/|\,p\,|)F(\gamma, \omega)f_E \tag{7}$$

in terms of fine-structure constant and the electron radius and momenta. The kinematic function $F(\gamma, \omega)$ is given explicitly by them, and to improve the results for the point Coulomb cases, as discussed by Lee, Kissel, & Pratt (1976) and by Pratt & Tseng (1975), we multiply $F(\gamma, \omega)$ by the Elwert factor f_E. These relativistically correct formulae depend on the composition of the plasma, which is model dependent. We approximate the thermal state at late times as a neutral atomic gas (actually about 4000 K in young supernova remnants) having mass fraction X_Z of element Z. For each Compton-electron initial kinetic energy E_k, we calculate (for the particle's entire deceleration) the fractional bremsstrahlung production in every frequency band, and these creation probabilities are then summed over all recoil electrons within a given mass element. That is, bremsstrahlung are not calculated as discrete photons by discrete Monte Carlo events, but rather as a smooth continuous production spectrum for each electron. Specifically we compute the bremsstrahlung power $W(\omega_1, \omega_2)$ in the frequency bin (ω_1 to ω_2) for each electron of initial energy E_k in depth-i's spectrum $n_e^i(E_k)$ (as in Fig. 1), and we integrate it over each increment of electron energy loss due to inelastic collisions from equation (5):

$$\begin{aligned} W^i(\omega_1, \omega_2) &= n_e^i(E_k)\int_{\omega_1}^{\omega_2}\int_0^{T_{\rm stop}}(dW/d\omega\, dt)d\omega\, dt \\ &= n_e^i(E_k)\int_{\omega_1}^{\omega_2}\int_{\hbar\omega}^{E_k}(dW/d\omega\, dt)d\omega[dE/(v\, dE/dx)]\,. \end{aligned} \tag{8}$$

When integrated in this way over photon frequency and over the continuously declining electron energy, the resulting ratio of total bremsstrahlung energy to the initial energy of the electron is obtained; it is traditionally called the *bremsstrahlung yield*. Its value is composition dependent, being mostly between 2–8 $\times$ 10^{-3} (ergs brems [ergs E_k]$^{-1}$). To check our computational prescription we compared for specific compositions our integrations with tabulations of bremsstrahlung yields (Pratt et al. 1977; ICRU Rept. 1984) and found them to be accurately reproduced. Figure 4 displays this comparison for the monoelemental materials Fe, O, and He, and for a 50% mixture of Fe and He. Our results from equation (8) are shown there as continuous curves and entries from Table 12.3 of ICRU Report 37 by points. The elemental yields show not only our agreement with Pratt et al. and ICRU tables, but also the

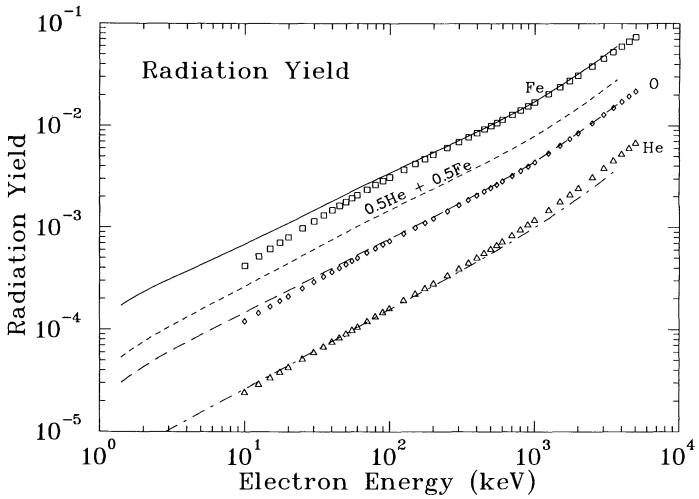

FIG. 4.—Bremsstrahlung yields during the entire stopping paths for electrons of given initial kinetic energy in elementally pure Fe, O, and He and in a 50% mix of Fe and He. Our calculations (shown as continuous curves) are compared with Table 12.4 of ICRU Report 37 (1984), which are the points. Yields (total bremsstrahlung energy per initial kinetic energy) increase with atomic number Z despite the associated increase in stopping cross section as well.

energy and elemental dependence of the bremsstrahlung yield, which will be of interest in their own right to other workers on this and related problems. The Z^2 dependence of the cross section results in a higher yield from Fe than for O, for example, despite the larger stopping power for Fe as well. As a consequence, supernova zones containing abundant Fe are better emitters than those without. Outward mixing of Fe in supernovae therefore can increase their bremsstrahlung luminosities below the K edge at 7 keV for this reason (as well as others); however, increased photoelectric opacity at frequencies above the K edge cause that part of the bremsstrahlung continuum to be reduced by the Fe photoabsorption by an amount greater than the increase of emissivity owing to the Fe. Model W7 below of a Type Ia explosion will illustrate this best, and we return to it there.

In the supernova models we record the depth beneath the surface of the scattered electron as well as its energy. The locally produced bremsstrahlung are calculated at each depth by summing over the spectrum of initial energies of the recoil electrons, an example of which was also shown as the smooth dashed curves in Figure 1. This smooth bremsstrahlung emissivity is then sampled by discrete Monte Carlo photons for purposes of evaluating their propagation through the model interior. That last computation evaluates the model luminosity.

For the SN 1987A model 10hmm of Pinto & Woosley (1988a, b), Figure 1 displayed not only the rate of Compton scatterings (*upper histograms*) but also the bremsstrahlung production rate per keV per gram at the same depths (*dashed curves*). The bremsstrahlung spectrum, varying with energy as $E^{-1.3}$, is seen to be virtually depth independent, a result of the interior electron-recoil spectrum being itself almost depth independent. The power law $E^{-1.3}$ is the natural result of bremsstrahlung physics and the spectrum of ^{56}Co gammas that initiates the energy cascade. It steepens to about E^{-2} near 1 MeV and truncates near 3 MeV, as do the recoil electrons. From Figure 1 it is also evident that the rates of Compton scattering and of associated bremsstrahlung production both

increase with depth. This reflects the increase of the intensity of primary radioactivity gammas with depth. The bremsstrahlung emissivity histograms are smooth and show no discernible statistical scatter, unlike the electron spectrum, because each electron itself produces a continuous emission probability between its total energy to zero energy as described above. Another 3 hr of Decstation 3100 CPU time was required to calculate the distributed bremsstrahlung emissivity for each model (a given structure at a given time). Analogous results will be displayed below for other types of supernova models, especially for a Type Ia exploding white dwarf.

5. BREMSSTRAHLUNG LUMINOSITY

How many bremsstrahlung emerge from the surface (the luminosity) is an altogether different question, and was addressed by Monte Carlo sampling. The optical depth from center to surface increases severely below 100 keV because of photoelectric absorption, as shown in Figure 9 of The et al. (1990a), so that lower energy photons must come from nearer the surface. We have evaluated the spectrum and flux of emerging bremsstrahlung for model 10hmm using a modified version of the Monte Carlo transport code described by The et al. (1990a). The analytic bremsstrahlung production at each depth is taken as a photon source for the random propagation of additional photons. This component of the hard-photon spectrum is thereby evaluated independently and identified. Because of the size of the computational problem at this point, we assumed the bremsstrahlung to be emitted isotropically. Results for bremsstrahlung emissivity per gram from specific depths are repeated in Figure 5 in order to show also the spectrum that emerges at the surface from that same interior gram. The same units apply to both curves, so that at high energy the emerging photons per gram tend asymptotically toward the produced photons per gram. The smallest production rate among the example depths shown there occurs from the depth nearest the surface, at optical depth $\tau_{20} = 0.29$ at $\hbar\omega = 20$ keV, which is located at 700 days at $m = 3.89\ M_\odot$ from the surface. But that depth dominates the others shown in the spectra emerging below $E = 10$ keV. Emerging spectra from the differing depths are shown as histograms whose statistical scatter again reflects the finite numbers emerging in each energy bin of the calculation and contrasts with the smoothness of the emissivity curves in the upper half. The stronger deeper production dominates the bremsstrahlung luminosity at higher energies, for which the photoelectric opacity is much smaller. Deep zones produce emergent spectra with maxima near 50 keV. Each emergent spectrum has a low-energy cutoff due to photoelectric absorption, but that cutoff moves down in energy for mass shells increasingly near the surface.

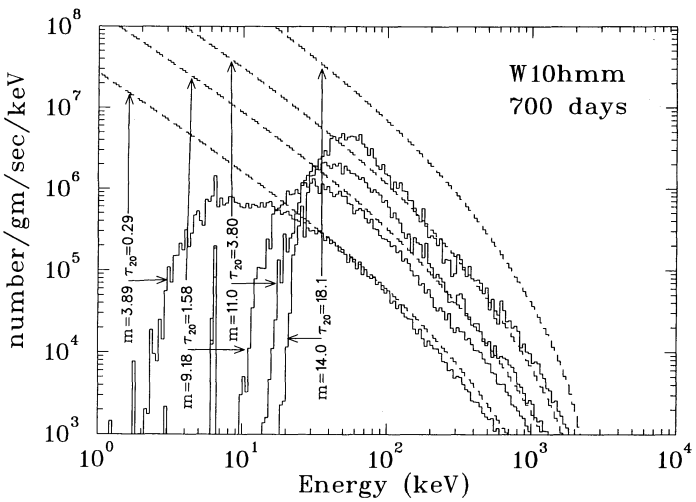

FIG. 5.—Smooth upper histograms repeat the bremsstrahlung emissivity per gram from the depths shown in Fig. 1. Mass m is the total (in $M_\odot$) from the depth to the surface, and τ_{20} is the optical depth at 20 keV. Lower histograms show the portion of that bremsstrahlung production which emerges from the surface of model 10hmm of SN 1987A as determined by Monte Carlo samples. Ordinate label applies to both sets, so the emerging spectrum tends at high energy toward the production spectrum. X-rays resulting from photoinduced K shell vacancies are also shown (see also Fig. 6). Each depth suffers a low-energy cutoff that moves upward in energy as the optical depth increases.

In Figure 6 we show the total photon spectrum (sum of scattered gammas, bremsstrahlung and K X-rays) at four separate times (175, 350, 700, and 1000 days) for model 10hmm of SN 1987A. The Monte Carlo transport histories of 3×10^5 bremsstrahlung photons shown for each panel required an additional 6 hr each of 3100 CPU time. Above about 25 keV the Compton-scattered gammas from radioactive decay dominate the spectrum. Below that energy the initial gammas dominate only at the 14 keV line from ^{57}Co decay. Below 20 keV the bremsstrahlung dominates (except for the 14 keV line and the Fe-group X-rays). The solid curve shows the sum of the two sources. We found the entire spectrum at early times to be more intense because the radioactivity source is then stronger and, for the bremsstrahlung, also because the production of fast electrons near the surface is then more efficient as well. Therefore, the bremsstrahlung luminosity is relatively more pronounced at day 350 in comparison with the almost unchanged 14 keV line from ^{57}Co and other nuclear lines at day 700, for example. The bremsstrahlung fraction of the continuum photon luminosity below 30 keV increases with time even though both bremsstrahlung and Comptonized gammas actually decline with time. The small cusps in the bremsstrahlung continuum at 8 keV (best seen at 700 and 1000 days) are the result of the jump in photoelectric opacity for photons above the Fe K edge at 7 keV.

6. K SHELL VACANCIES CREATED BY PHOTONS

Atomic inner-shell lines also contribute to the photon luminosity below 7 keV; and their emissivity derives from all inelastic collisions that create K shell vacancies. These collisions are (1) with recoil electrons, (2) Compton scattering, and (3) from photoelectric absorption, both from the Comptonized gammas and from the created bremsstrahlung. Photoelectric absorption of Comptonized gammas is for the heavy elements the most important such collision. For the important K X-ray line energy (about 6.4 keV) of Fe, the photoelectric collisions dominate the other processes in the production of K shell vacancies, but in lighter elements collisions with the recoil electrons, absorption of bremsstrahlung, and Compton scattering may be more important. For Fe, fast electrons are more important than bremsstrahlung because, in an Fe-rich gas, one must inject $\sim$20 70 keV electrons to obtain one K shell vacancy collisionally (The et al. 1991), whereas one must inject $\sim$170 such electrons to create one bremsstrahlung photon above 8 keV energy. For the lighter elements, on the other hand, photoelectric absorption of bremsstrahlung dominates that of gammas, but in those cases the inelastic collisions with recoil electrons (The et al. 1991) and Compton scattering of gammas are the dominant creators of K shell vacancies. Bremsstrah-

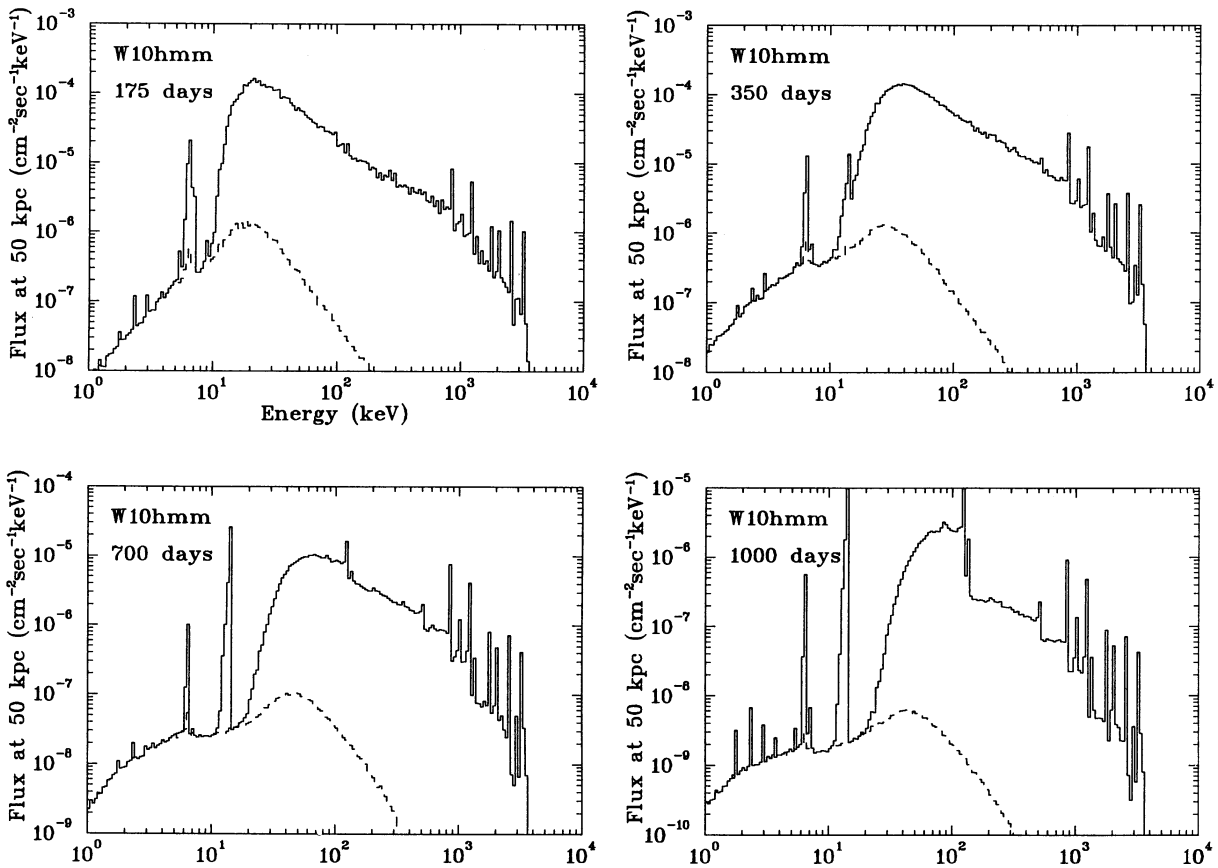

FIG. 6.—Photon continuum flux per keV (including X-Ray and gamma line contributions) at 50 kpc from model 10hmm of SN 1987A. The four panels show the four times 175, 350, 700 and 1000 days. Solid histogram is the sum of primary photons from cobalt decays and secondary bremsstrahlung from recoil electrons (*dashed*). Primary photons dominate above 20 keV and bremsstrahlung below 20 keV (except for 14 keV and K X-rays). Bremsstrahlung escape declines only slowly toward lower energies, roughly $F(v) \propto v^n$ with $n = 1$–1.5 for most models studied in this work, because production is peaked toward low energy. Emergent photons are binned logarithmically in 188 bins between 1 keV and 4 MeV, specific bin boundaries being $E_i(\text{keV}) = 10^{0.02(i-2)}$ for $i > 1$, so line fluxes from ^{56}Co decays are the product of histogram height and bin energy width $\Delta E_i = E_{i+1} - E_i$. The nuclear lines are identical to the fluxes calculated by The et al. (1990a), but the K X-rays due to photon-induced K shell vacancies are calculated in this work. The energy bins necessary for converting these continuum fluxes (per keV) to line X-ray fluxes are given above. The *Ginga* 16–28 keV band is on falling portion of the primary spectrum (the photoelectric cutoff) and is therefore sensitive in a different way than the bremsstrahlung to the treatment of model details.

lung do not, therefore, dominate the K shell vacancies of any element within the interior, despite dominating the radiative vacancy rate for light elements, but their importance to circumstellar ionization is higher. A numerical example is found in the final paragraph of this section.

Each of these inelastic processes is partly responsible for the K X-ray Fe line in SN 1987A (Tanaka 1988). We defer our full treatment of the collisions with the recoil electrons to a subsequent work (The et al. 1991). Both Compton scattering and photoelectric absorption contribute heavily to K shell vacancies deriving from the Comptonized gamma spectrum. Xu et al. (1988) and Pinto & Woosley (1988b) have already calculated and discussed the K X-rays of Fe produced by the Comptonized gamma rays. Inelastic electrons and bremsstrahlung photoelectric absorption are also partly responsible for the strong He excitation (Graham 1988) within SN 1987A outflow. To calculate that ionization state requires inclusion of all of these processes. We will publish our full calculations of these for all the major elements in the work to follow. The reader will be interested to know one conclusion, however, namely, the bremsstrahlung luminosity of a model is almost independent of uncertainties concerning the magnitude of the low-energy portion (20 keV $< E <$ 40 keV) of the continuous Comptonized spectrum, whereas the K X-ray line luminosities are sensitive to those uncertainties.

We have displayed in this work our calculations only of those K X-rays created by *photon-induced K-shell vacancies*, both in Figure 5 showing the photon spectrum emerging from selected depths within model 10hmm of SN 1987A and in Figure 6 showing the total luminosity of model 10hmm of SN 1987A. Those K X-rays also appear on emission spectra from other models of supernovae to be discussed below. The 6.4 keV X-ray from Fe is very prominent in the calculated 700 day spectrum (and later) of SN 1987A. K X-rays from Co, Cr, Ar, S, Si, and Mg are also evident in Figure 6. Our subsequent work (The et al. 1991) will document the increase of each of these K X-rays due to the inelastic collisions with Compton-recoil electrons. Because our figures display continuous spectra (keV^{-1}), the line fluxes are recovered by multiplying the line peaks shown on the histograms by the energy bin width used in our calculations. Those energy bins (in keV are $\Delta E_i = E_{i+1} - E_i$, with the bin boundaries being $E_i(\text{keV}) = 10^{0.02(i-2)}$ for $i > 1$.

In some of our calculations we have decomposed the parentage of these X-rays according to (1) photoelectric absorption of

gammas; (2) photoelectric absorption of bremsstrahlung, and (3) Compton scattering of gammas. The importance of bremsstrahlung is easy to discern from such a procedure but hard to visualize otherwise. Bremsstrahlung are increasingly more important for decreasing atomic number, but so too is Compton scattering as a source of K shell vacancies. An example will have to suffice—from a shell 6 $M_\odot$ inward from the surface of 10hmm at $t = 500$ days. At that time and place the photoelectric absorption of bremsstrahlung exceeds that of Comptonized gammas only for He, is roughly equal for C, and 40 times smaller for Fe. For Fe the photoelectric effect creates 100-fold more K vacancies than does Compton scattering, whereas for O the two rates are about equal, and for He the Compton effect dominates. Bremsstrahlung are not dominant for any element, but we have found and will report later (The et al. 1991) that the Compton-recoil electrons presented by us (Fig. 1) are more important than any photon process in the creation of K shell vacancies for elements lighter than Si. For Fe the photon absorption dominates. Thus the total picture is complicated. Further remarks on the importance of bremsstrahlung will be found later in our presentation of a Type Ib model, where the intense spectrum contributes more.

7. SUMMARY OF 10HMM APPLICATIONS

An important physical feature decouples both the bremsstrahlung luminosity (and that in X-ray lines) to some degree from the continuous luminosity of the scattered gammas. The latter emerge from deeper zones than do the former two. To see this by concrete example, consider the ratio of 14 keV bremsstrahlung to the 14 keV line from ^{57}Co. Even though the 14 keV line and Comptonized 14 keV continuum may be unable to escape from the core containing the radioactivity because of the large photoelectric absorption between that core and the surface, X-rays of the same energy can escape if they are created nearer the surface. Bremsstrahlung are capable of exactly such near-surface production as the result of the energetic electrons created by scattering of higher energy gammas near the surface. Our basic finding is that this bremsstrahlung creation of a 14 keV quantum is much more probable than the downscatter of a gamma to 14 keV—at least for those photons that emerge from the surface. This emphasis on near-surface layers renders the ratio bremsstrahlung/gammas model dependent in very interesting ways.

Table 1 summarizes the following model 10hmm evaluations: total recoil-electron kinetic energy rate KE_C; average recoil energy $\langle KE_C \rangle$ per recoil electron for those scatterings having E_k greater than 1 keV (shown, however, by an average bar in the tables); bremsstrahlung yield from KE_C; total bremsstrahlung power E_{brem} created within the interior; number fluxes F^{brem}_{1-10}, F^{brem}_{10-20}, and F^{brem}_{20-30} at Earth from escaping bremsstrahlung (i.e., not including Fe K X-ray and the ^{57}Co line at 14 keV). The ratio of F^{brem}_{20-30} to the Comptonized gammas in the same band (not shown in Table 1) increases with time. These fluxes are for the known distance 50 kpc, unlike those for other types of events (below) which take a nominal 1 Mpc distance. All Type II supernovae are characterized by lower average recoil energy $\langle KE_C \rangle$ than are Type Ia and Type Ib supernovae (compare below), because the more massiver envelopes of Type II cause many more multiple scatterings, which are of necessity of low average recoil energy. The rate of Compton events is clearly the ratio of KE_C and $\langle KE_C \rangle$.

Several results seem significant for astronomy. First, X-ray detectors could in principle measure the X-ray luminosity of SN 1987A in the keV region that is dominated by bremsstrahlung luminosity. The expected value is sufficiently sensitive to the details of the supernova model and its opacity that we cannot here make a prediction more firm than indicated by the results Figure 7 and in Table 1. The luminosity in 1990 July ($t = 1250$ days) and in 1990 March ($t = 1500$ days) is calculated by us to be only 7.4×10^{28} ergs s^{-1} and 2.6×10^{28} ergs s^{-1}, respectively, in the range 0.1–2 keV. This is much less than the *ROSAT* upper limit (not yet published) in that energy range.

While discussing bremsstrahlung luminosity, we note also that the keV X-rays measured at earlier times by *Ginga* have already been differently interpreted, namely as a circumstellar luminosity due to collision between the rapid ejecta and circumstellar matter (Masai et al. 1988; Spicer, Clark, and Maran 1990), so the path to the correct interpretations may take some time. That entirely different process depends upon additional conditions, whereas the one we present, from the supernova interior, requires no added assumptions, but must be present. Because of the ω^{-3} dependence of photoelectric opacity on frequency, even the relatively low bremsstrahlung luminosity below 20 keV can be significant to inner-shell ionization balance within both ejecta and circumstellar material. The fast electrons themselves will also be important to that balance and to the abundance of molecules such as CO in the outflow (Lepp, Dalgarno, & McCray 1990). Therefore, many readers will find these calculations to be relevant.

Late-time luminosities of 10hmm at 1250 and 1500 days are shown in Figure 7 and were included in Table 1. For these two late times the ^{44}Ti radioactivity was also included, so that technically it is not the exact same calculation as for Figure 6. Woosley et al. (1989) discussed the relevance of ^{44}Ti for the late-time light curve. We gave it an abundance relative to ^{56}Fe

TABLE 1

MODEL W10hmm CHARACTERISTICS

Time (days)	KE_C (ergs s^{-1})	$\overline{KE_C}$ (keV)	Yield$_{brem}$ (10^{-3})	E_{brem} (ergs s^{-1})	F^{brem}_{1-10} [a] (cm^{-2} s^{-1})	F^{brem}_{10-20} [a] (cm^{-2} s^{-1})	F^{brem}_{20-30} [a] (cm^{-2} s^{-1})
175.....	2.11×10^{41}	94.1	1.76	3.72×10^{38}	1.89×10^{-6}	1.03×10^{-5}	1.07×10^{-5}
350.....	3.86×10^{40}	104	1.51	5.81×10^{37}	2.50×10^{-6}	6.55×10^{-6}	1.21×10^{-5}
500.....	8.09×10^{39}	120	1.93	1.56×10^{37}	1.05×10^{-6}	2.02×10^{-6}	3.51×10^{-6}
700.....	9.82×10^{38}	123	2.12	2.08×10^{36}	1.90×10^{-7}	3.23×10^{-7}	5.45×10^{-7}
1000.....	4.26×10^{37}	69.3	1.45	6.18×10^{34}	1.29×10^{-8}	2.28×10^{-8}	3.77×10^{-8}
1250.....	6.02×10^{36}	31.3	1.16	6.99×10^{33}	1.84×10^{-9}	3.18×10^{-9}	5.29×10^{-9}
1500.....	1.81×10^{36}	22.9	0.655	1.18×10^{33}	5.54×10^{-10}	9.17×10^{-10}	1.40×10^{-9}
2000.....	5.05×10^{35}	28.6	0.735	3.71×10^{32}	2.33×10^{-10}	4.72×10^{-10}	8.00×10^{-10}

[a] Assuming distance of 50 kpc and no interstellar absorption.

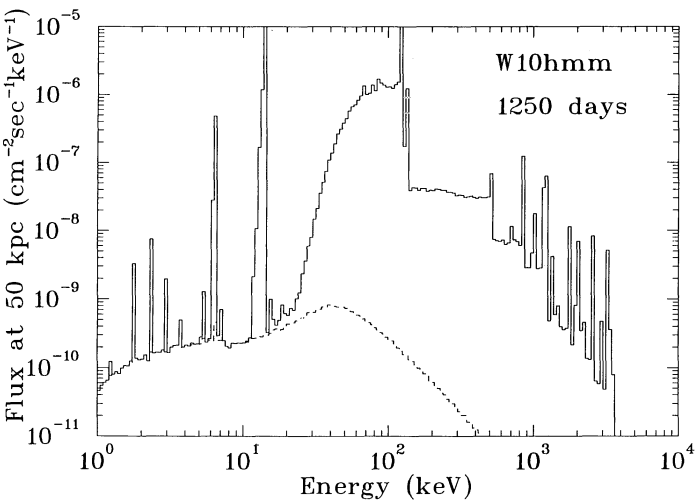

FIG. 7a

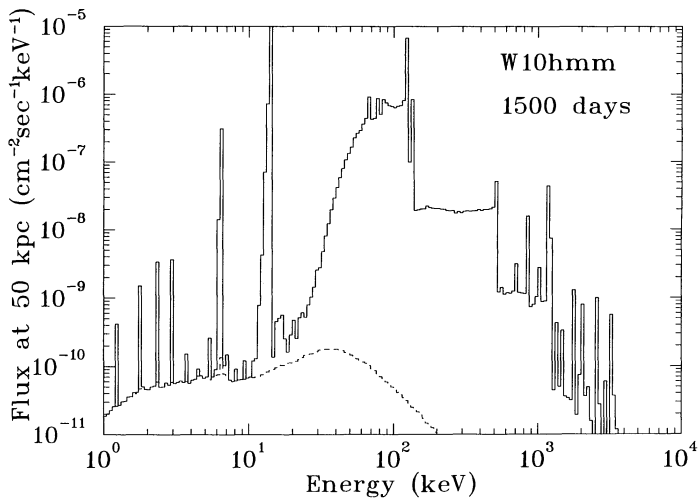

FIG. 7b

FIG. 7.—The photon spectrum of 10hmm at (*a*) 1250 days and (*b*) 1500 days. Format and calculation are as in Fig. 6. Bremsstrahlung continuum is the dashed curve between 1–200 keV underlying the X-ray line spectrum. The X-rays evident clearly are Co (6.93 keV), Fe (6.40 keV), Cr (5.42 keV), Ca (3.69 keV), Ar (2.96 keV), S (2.31 keV), Si (1.74 keV), and Mg (1.26 keV). The ^{44}Ti radioactivity was added to the sources for these late times. The luminosity in the *ROSAT*-sensitive band 0.1–2.0 keV is (*a*) 7.4×10^{28} ergs s^{-1}, (*b*) 2.6×10^{28} ergs s^{-1}, considerably smaller than the detectable threshold of that instrument but hundreds of times greater than the Comptonized gammas in the same energy band.

that is solar, but its true value is uncertain. Almost the only effect of ^{44}Ti that can be seen by the eye in Figure 7 is the doublet 68 and 78 keV from the ^{44}Ti decay, and an increased strength at 1.16 MeV from the subsequent ^{44}Sc decay. Small effects at 511 keV and in the cutoff of the Compton tail of gammas are also there, but not easily discernible. Otherwise the calculations are identical. Of particular interest to the present work is the X-ray luminosity from the bremsstrahlung and its comparison with *ROSAT* observations. Unfortunately, *ROSAT* appears to not see SN 1987A because it is so faint in X-rays; however, our predictions can be seen to be a large factor beneath the upper limits near 10^{33} ergs s^{-1} set by them. Our results for the X-ray luminosity in the energy band 0.1–2.0 keV for 10hmm are $L(1250 \text{ days}) = 7.4 \times 10^{28}$ ergs s^{-1}; $L(1500 \text{ days}) = 2.26 \times 10^{28}$ ergs s^{-1}; $L(2000 \text{ days}) = 1.2 \times 10^{28}$ ergs s^{-1}. As faint as our predictions are, they are of unusual interest in that they must be there. No ad hoc assumptions are required. They are completely due to bremsstrahlung emitted by the Compton-recoil electrons. These X-ray luminosities are the smallest SN 1987A can have and still be consistent with the theory of the radioactivity-powered light curve.

8. MODEL SN 11E1 OF SN 1987A

The foregoing results were illustrated with the aid of model 10hmm of SN 1987A. We also evaluated another model of that event, model SN 11E1 (Nomoto et al. 1988; Kumagai et al. 1989). It has been shown by them and by The et al. (1990a) to have gamma-ray-line light curves almost identical to 10hmm. We reconfirm that result with new calculations. Figure 8 shows the spectral flux from SN 11E1 at the same 4 times as in Figure 6. Consistent with the equality of their high-energy spectra, the lower energies, F^{brem}, are also virtually the same as for 10hmm. Table 2 lists the global characteristics of SN 11E1 in the same format used for Table 1. Below the Fe X-ray line at 6.4 keV, SN 11E1 is about half as luminous as 10hmm, but their spectra are virtually identical above 10 keV. Not surprisingly we conclude that models that are constructed to fit both bolometric light curves and gamma-ray-line light curves of SN 1987A will not be easily distinguished by bremsstrahlung luminosity or K X-ray luminosity, even if those can be detected. The spectra of recoil electrons are very similar to those in Figure 1 and are therefore not shown; however, small differences in bremsstrahlung emissivity from those in Figures 1 and 2 are evident in

TABLE 2

MODEL SN 11E1 CHARACTERISTICS

Time (day)	KE_C (ergs s^{-1})	$\overline{KE_C}$ (keV)	Yield$_{\text{brem}}$ (10^{-3})	E_{brem} (ergs s^{-1})	F^{brem}_{1-10} [a] (cm^{-2} s^{-1})	F^{brem}_{10-20} [a] (cm^{-2} s^{-1})	F^{brem}_{20-30} [a] (cm^{-2} s^{-1})
175	2.12×10^{41}	98.9	1.97	4.17×10^{38}	1.10×10^{-6}	8.33×10^{-6}	1.12×10^{-5}
350	3.86×10^{40}	106	1.95	7.51×10^{37}	1.73×10^{-6}	5.99×10^{-6}	1.23×10^{-5}
500	7.80×10^{39}	126	1.98	1.54×10^{37}	8.28×10^{-7}	2.08×10^{-6}	3.74×10^{-6}
700	8.89×10^{38}	143	2.04	1.82×10^{36}	1.81×10^{-7}	3.84×10^{-7}	6.19×10^{-7}
700_{core}	8.76×10^{38}	124	2.05	1.79×10^{36}	2.52×10^{-7}	1.54×10^{-6}	3.44×10^{-6}
700_{env}	8.81×10^{38}	142	2.04	1.79×10^{36}	3.64×10^{-7}	4.51×10^{-7}	6.31×10^{-7}
1000	3.98×10^{37}	71.6	1.90	7.54×10^{34}	1.15×10^{-8}	2.25×10^{-8}	3.89×10^{-8}

[a] Assuming distance of 50 kpc and no interstellar absorption.

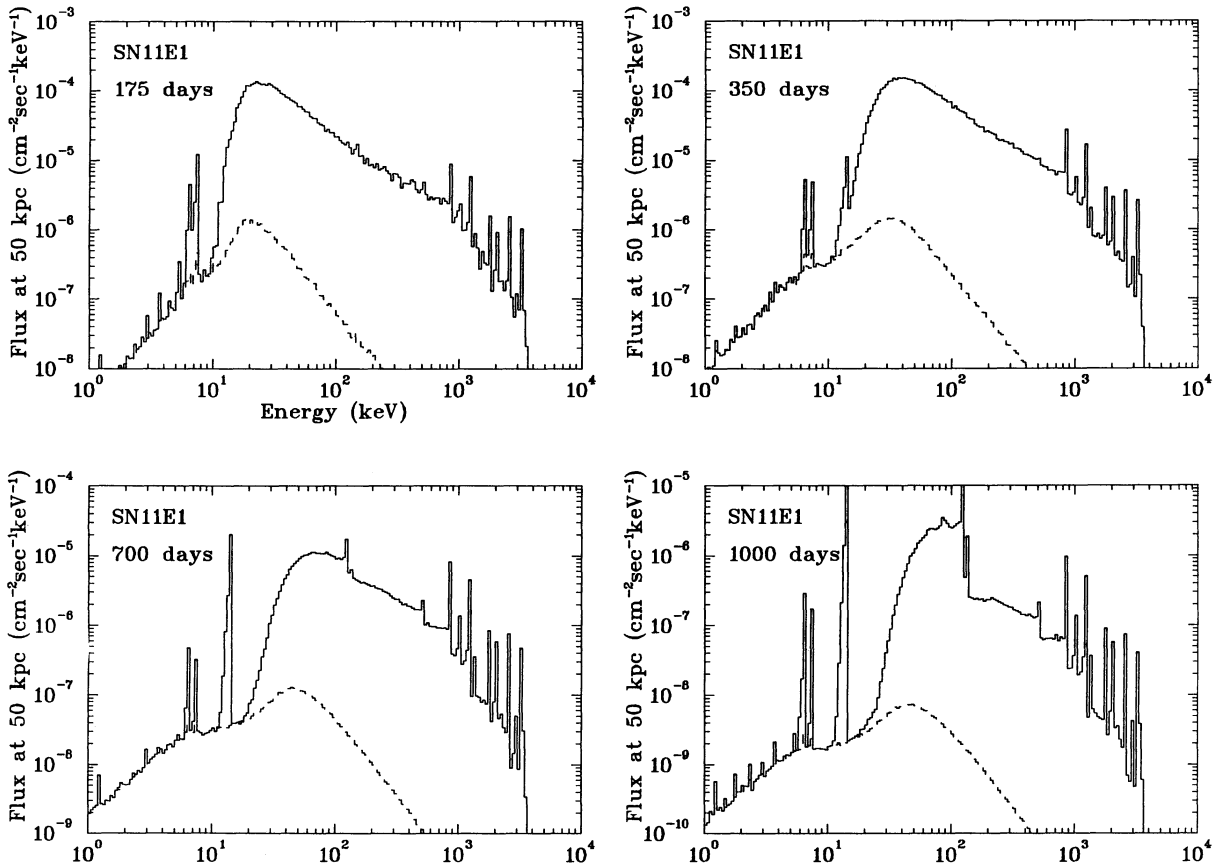

FIG. 8.—Flux per keV from model SN 11E1 of SN 1987A. Format is identical to Fig. 6, from which only small differences can be seen. Most evident difference is the strong Ni X-ray line at 7.48 keV from SN 11E1, which exists because the nucleosynthesis of ^{58}Ni was included in our SN 11E1 file but not in that of 10hmm. Differences in atomic K X-rays and in bremsstrahlung reflect differences in the mixing of nucleosynthesis products (Fe, etc.) outward.

those zones for which the two models have different compositions because of the slightly differing bremsstrahlung yields.

The discerning eye can see small but interesting differences between SN 11E1 and 10hmm, however. Most visible is the strong K X-ray of Ni in 11E1 at 7.5 keV. This comes from ^{58}Ni synthesized in the explosion and mixed outward with the Co, as expected from general principles of nucleosynthesis (Clayton & Woosley 1969; see their Fig. 5) from silicon-burning shells. Its detection relative to that of iron can place important constraints on the details of nucleosynthesis. That ^{58}Ni nucleus was included in the 11E1 file, so its X-ray appears as a strong "doublet" with that of Fe at 6.4 keV in Figure 9, but it is missing from 10hmm (see Fig. 6) because it was not included in the abundances of the file on that model. This is not, therefore, a true difference. At low energies one may also notice that the 10hmm bremsstrahlung are slightly more luminous than 11E1's, as are also its K X-rays. This modest difference reflects differences in mixing of the X-ray–emitting intermediate-mass nuclei and of the resulting modification of the surface photoelectric opacity.

8.1. *Modified Photoelectric Opacity: Envelope*

We took this study as an opportunity to confirm a very interesting modification of the model opacity suggested by Kumagai et al. (1989). They discussed the difficulty in matching light curves, gamma lines, and *Ginga* hard-X-ray band at 16–28 keV (Tanaka et al. 1988) with any spherical uniform model of

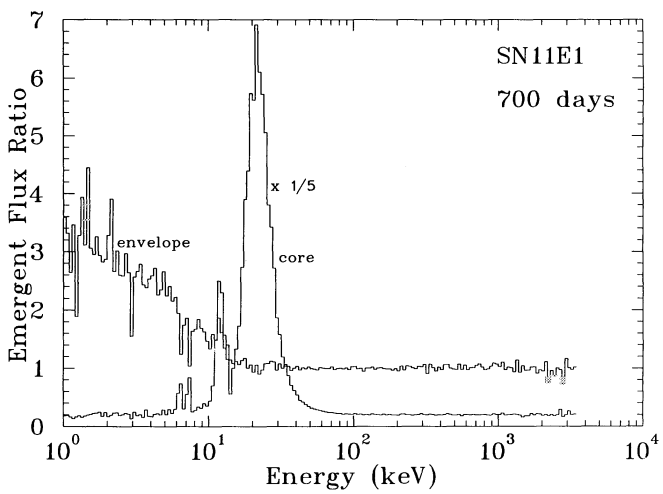

FIG. 9.—Spectral enhancement factors for opacity-change experiments measure the factor by which the total luminosity (Comptonized gammas + bremsstrahlung) of SN 11E1 was increased because of that change. Histogram labeled "envelope" was a factor of 3 reduction of the opacity in the outer 6 $M_\odot$ of the model, and that labeled "core" was a factor of 10 reduction of the inner 6 $M_\odot$. The reduction of envelope opacity increases only the lowest energy luminosity because it originates from the surface layers only, whereas the core-opacity reduction greatly increases the Comptonized-gamma luminosity in the 16–30 keV band that emerges from the core. The latter confirms the finding (Kumagai et al. 1989) that the hard *Ginga* band might be accounted for by a core-opacity reduction, probably due to clumping of the metals.

SN 1987A. We here present not only confirmation of one of their surprising results but also enlarge it to include the bremsstrahlung component. Kumagai et al. presented the interesting argument that reduction of the photoelectric opacity in the core would greatly increase the 16–28 keV band flux, whereas decreasing that opacity in the envelope would be ineffective in doing so. They argued that clumping of the core heavy metals could reduce the effective photoelectric optical depth of the core by a factor of 10, thereby increasing the *Ginga* band flux by reducing its photoelectric cutoff from the core. While confirming both of these dependences, we point out that for the bremsstrahlung emission, which is a secondary process, a reduction of the envelope opacity is also effective. To show this we calculated the 700 day spectrum of SN 11E1 with an arbitrary reduction by a factor 3 of the photoelectric opacity (only) in the outer $m = 6\ M_\odot$. Comparison of those results, which are included in Table 2 as "$700_{\rm envelope}$," are shown in Figure 9. The ratio by which the total flux (Comptonized gammas + bremsstrahlung) is increased by opacity change is plotted, and it confirms that the bremsstrahlung flux just above 1 keV is thereby increased by the same factor 3, just as one might expect. That increase declines steadily as energy approaches 10 keV, and the luminosity above 20 keV is totally unaltered by this change. Significant scatter from 1–10 keV is statistical, resulting from the small numbers of photons in the Monte Carlo energy bins used to transport these bremsstrahlung. Table 2 shows that the band $F^{\rm brem}_{1-10}$ was approximately doubled by this change whereas the band $F^{\rm brem}_{20-30}$ was hardly increased at all. Many factors could in fact reduce the envelope opacity from the value we used in our model, because a uniformly distributed neutral atomic gas has the largest possible photoelectric opacity. Factors that might reduce it include (1) clumping of those metals that were mixed from the core into the envelope; (2) clumping of the envelope into neutral clouds imbedded in a hot ionized matrix of lower density; (3) ionization of H and He, elements which contribute to the surface photoelectric opacity in our code but might not in reality; (4) tendency of bremsstrahlung to be somewhat radially emitted rather than isotropic, simulating a smaller average optical depth. Clearly our idealized results underestimate the bremsstrahlung luminosity, and the arbitrary factor 3 was chosen to probe that reduction.

8.2. *Modified Core Photoelectric Opacity*

We have also tested Kumagai et al.'s (1989) assertion that a smaller photoelectric opacity in the Co-rich core, which they attributed to clumping of the Fe-peak metals into cloudlets imbedded in lower Z admixed material, greatly increases the *Ginga* flux in its 16–28 band. We reduced that portion of the opacity in the inner $m = 6\ M_\odot$ by a factor 10 and repeated the calculations. Not only did the 16–28 band increase dramatically, but it did so more than any other portion of the spectrum, which was mostly unchanged! Both 10–20 keV and 20–30 keV bremsstrahlung bands, $F^{\rm brem}$ in the "$700_{\rm core}$" line of Table 2, were also increased markedly. This sensitivity to core photoelectric opacity arises from the fact that the 15–30 keV energy range lies on a portion of the emerging spectrum that is being cut off by photoelectric opacity. This can be seen more clearly in Figure 9, where we plot at 700 day the ratio by which the total continuous emission is increased by both of the above opacity reductions, with the core reduction labeled "core" and the envelope reduction by a factor 3 by "envelope." The factor of 35 increase near 20 keV for the core reduction is clearly the most sensitive one in the entire structure to these experiments, and that dramatic behavior happens to lie squarely in the middle of the *Ginga* band. This increase is largely due to the Comptonized gammas, but, as Table 2 shows, the bremsstrahlung component $F^{\rm brem}$ is also increased in the bands 10–20 keV and 20–30 keV. The 14 keV ^{57}Co line flux is increased too, as Figure 9 shows, but only by the smaller factor 12. The remainder of the spectrum is almost insensitive to such a change. The envelope-opacity reduction, on the other hand, increases the luminosity only at low energy—by a factor 3 (the reciprocal of the envelope opacity reduction) near 1 keV and by continuously declining factors at higher energy. This increase is of the bremsstrahlung component, which dominates the 1–10 keV continuum. This result is very easily understood. Reduction of the photoelectric opacity by a factor 3 allows the outside to see threefold deeper in column mass. This increases the luminosity only at those frequencies whose emission is entirely from the surface layers so involved, i.e., at low energy.

9. TYPE Ia SUPERNOVAE

We evaluate the same bremsstrahlung emission processes in Type Ia supernovae by utilizing a specific model of those objects. Here the differences are more dramatic, as one expects. Model W7 of Nomoto, Thielemann, & Yokoi (1984) has already been evaluated for its gamma-ray light curves by Burrows & The (1990; see their Fig. 7), so we considered it to be a good comparison case for which we already had the model file. Figure 10 shows the results for the spectral rate of Compton recoils and the bremsstrahlung emissivity (eq. [8]) per gram at three distinct depths within W7 at $t = 20$ days. It is the Type Ia analog of Figure 1 for SN 1987A, and one notices at once the roughly 10^4 times higher intensity levels. It is also evident that the electron-recoil spectrum is flatter out to higher energy. Quantitative evidence of this can be seen in two ways: (1) Table 3 listing the global characteristics of W7 shows the average recoil energy $\langle {\rm KE_C} \rangle = 158$ keV at 20 days and increasing to 300 keV by 80 days, whereas in SN 1987A models $\langle {\rm KE_C} \rangle$ is only about 100 keV. At first sight this seems surprising since both are driven by the same ^{56}Co spectrum of gammas. But the explanation is to be found in the higher

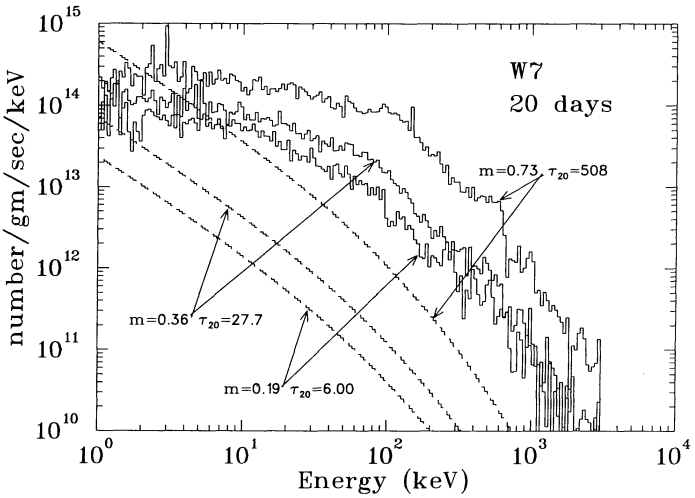

FIG. 10.—Production rate per gram of recoil electrons per keV at distinct depths in model W7 of a Type Ia supernova at $t = 20$ days. Depths are shown in $M_\odot$ from the surface and in optical depth at 20 keV to the surface, exactly as in Fig. 1 but about 10^4 times more intense.

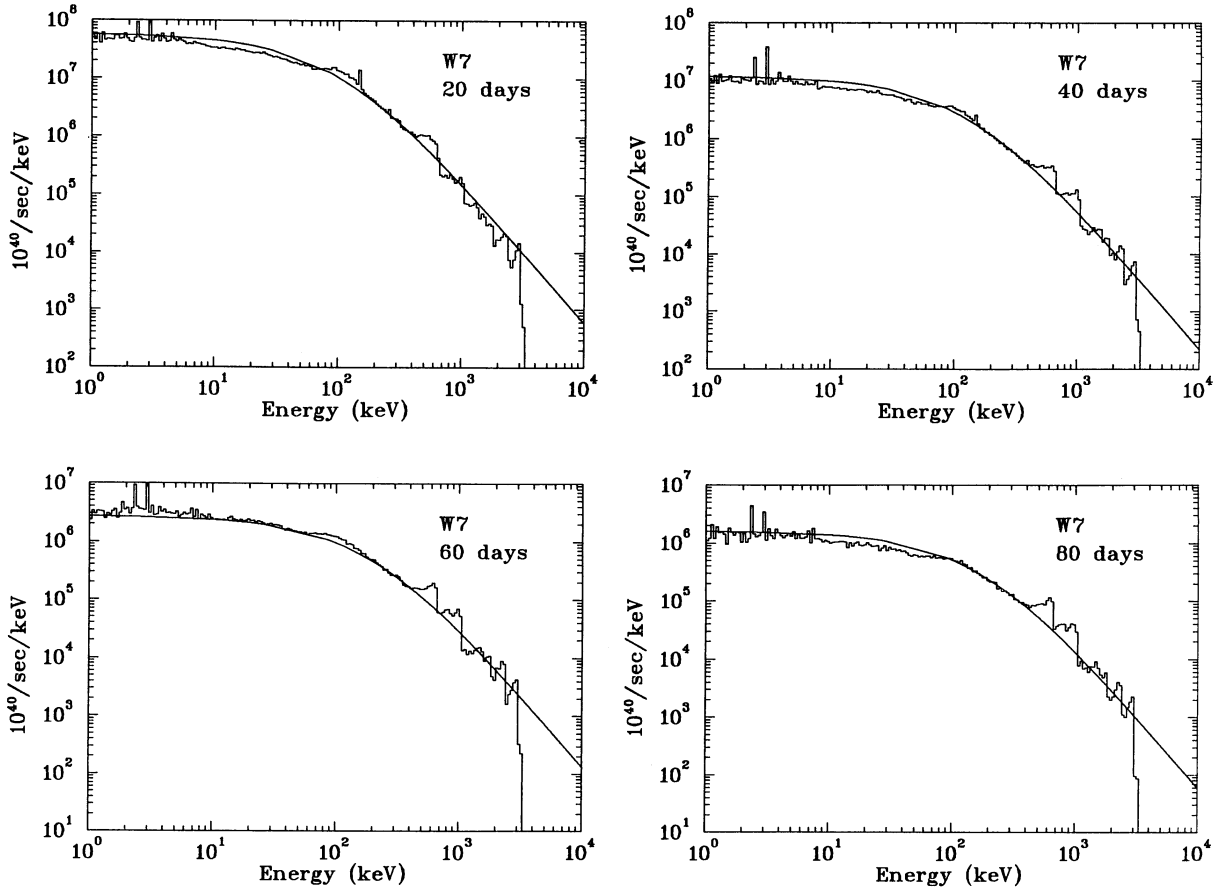

FIG. 11.—Comparisons of the mass-integrated Compton-recoil spectrum within model W7 (Type Ia) with the approximate fitting function as in Fig. 2. But in this case the exponent for the energy-break power law is $(1 + E/E_0)^{-2.5}$ for all panels (instead of 2.0 as in Fig. 2) and the breakpoint energy E_0 is for the four times shown 101, 129, 192, and 171 keV, in increasing temporal order. The much larger energy E_0 reflects the flatness of the recoil spectrum to much higher energy in this Type Ia model than in the SN 1987A models.

number of scatterings *per gamma* in SN 1987A. Photons that scatter twice, for example, produce much smaller $\langle KE_C \rangle$ than ones that scatter only once. We have tagged our emerging spectra with code modifications that display the number of scatterings that were involved in the production of each emerging photon, and these results confirm this interpretation. However, we choose to not get into those interesting results here. (2) Another evidence of the relative hardness of the Type Ia electron spectra is in Figure 11, which shows the global fits to the recoil spectra at four times. In this Type Ia analog of equation (3) constructed for SN 1987A, the factor $(1 + E/E_0)^{-2.5}$ has both a larger exponent ($n = 2.5$ instead of 2.0) and a larger value of E_0 as well as the larger value for $\langle KE_C \rangle$. We again find that the same exponent (2.5 in this case) can be used for all four times, but the best-fit values for E_0 are 101, 129, 192, and 171 keV, respectively, for increasing time. Curiously, the bremsstrahlung emissivity of Figure 10 still has the power-law slope $E^{-1.3}$ below 100 keV. This constancy is the natural result of the dominance of the highest energy recoils on the bremsstrahlung emissivity.

Figure 12 shows, in direct analogy with Figure 5, the relationship between the bremsstrahlung emissivity at those same four depths and the spectrum that actually emerges from the surface from those depths. Note that the optical depths at 20 keV, which also label the zones, are quite large at 20 days. The emissivity is again smooth because of the distributed production of each electron, whereas the emerging spectrum has statistical scatter resulting from the Monte Carlo propagation of the emissivity through the model W7. The shallowest zones again dominate the luminosity at the lowest emerging energies

TABLE 3

MODEL W7 CHARACTERISTICS

Time (days)	KE_C (ergs s^{-1})	$\overline{KE_C}$ (keV)	$Yield_{brem}$ (10^{-2})	E_{brem} (ergs s^{-1})	$F^{brem\ a}_{1-10}$ ($cm^{-2}\ s^{-1}$)	$F^{brem\ a}_{10-20}$ ($cm^{-2}\ s^{-1}$)	$F^{brem\ a}_{20-30}$ ($cm^{-2}\ s^{-1}$)	$F^{brem\ a}_{30-40}$ ($cm^{-2}\ s^{-1}$)	$F^{brem\ a}_{40-50}$ ($cm^{-2}\ s^{-1}$)	$F^{brem\ a}_{50-60}$ ($cm^{-2}\ s^{-1}$)
20.....	9.59×10^{42}	158	1.08	1.04×10^{41}	7.78×10^{-8}	4.97×10^{-7}	1.04×10^{-6}	1.54×10^{-6}	2.25×10^{-6}	3.03×10^{-6}
40.....	3.47×10^{42}	218	1.36	4.72×10^{40}	2.26×10^{-7}	9.96×10^{-7}	1.56×10^{-6}	2.21×10^{-6}	2.97×10^{-6}	3.47×10^{-6}
60.....	1.68×10^{42}	266	1.50	2.51×10^{40}	2.43×10^{-7}	8.69×10^{-7}	1.44×10^{-6}	2.03×10^{-6}	2.54×10^{-6}	2.97×10^{-6}
80.....	8.77×10^{41}	298	1.50	1.32×10^{40}	2.31×10^{-7}	7.75×10^{-7}	1.26×10^{-6}	1.74×10^{-6}	2.11×10^{-6}	2.44×10^{-6}

[a] Assuming distance of 1 Mpc and no interstellar absorption.

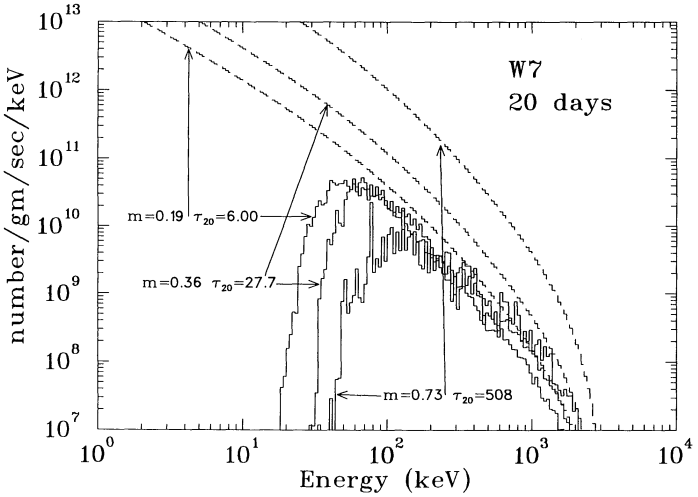

FIG. 12.—Comparison at $t = 20$ days for model W7 (Type Ia) of the bremsstrahlung emissivity per gram at three separate depths with the surface luminosity from the same depths, which are the same depths as in Fig. 10. The emissivity varies as $E^{-1.3}$. Surface luminosity is severely cut off because of the large optical depths (shown for 20 keV X-rays) to these mass shells. Shallower depths contribute more to the lowest emerging energies.

(<100 keV), but the contributions above 100 keV are more equally distributed in depth. Each emerging spectrum has its own low-energy photoelectric cutoff that is quite abrupt and that moves up in energy as one moves down into the model.

Figure 13 shows the total spectral luminosity of W7 at four times, 20, 40, 60, and 80 days after explosion. The gamma lines and the Comptonized continuum are identical to the earlier calculations of Burrows & The (1990), as they should be since they used the same program. But all of the modifications described in §§ 1–6 were also included. Very evident is the robust bremsstrahlung luminosity between 1 and 10^3 keV, with a maximum near 100 keV. Below that maximum, the photoelectric opacity progressively consumes the emitted bremsstrahlung, causing lower luminosity at lower energy, but does not do so as severely as it does the Compton tail of the gammas, which plunges sharply at an energy near 100–60 keV. At $t = 40$ days, for example, the bremsstrahlung and Comptonized gammas have equal luminosity at 50 keV, with bremsstrahlung dominating below that. This flux at 1 Mpc from a Type Ia would perhaps be detectable by the OSSE spectrometer aboard *GRO* (Johnson et al. 1989), which is expected to have a flux limit near 10^{-7} cm^{-2} s^{-1} keV^{-1} near 50 keV. The change of slope near 50 keV constitutes a subtle diagnostic.

Despite the strong bremsstrahlung luminosity, only 12% of circumstellar Si atom K shell vacancies are created by them,

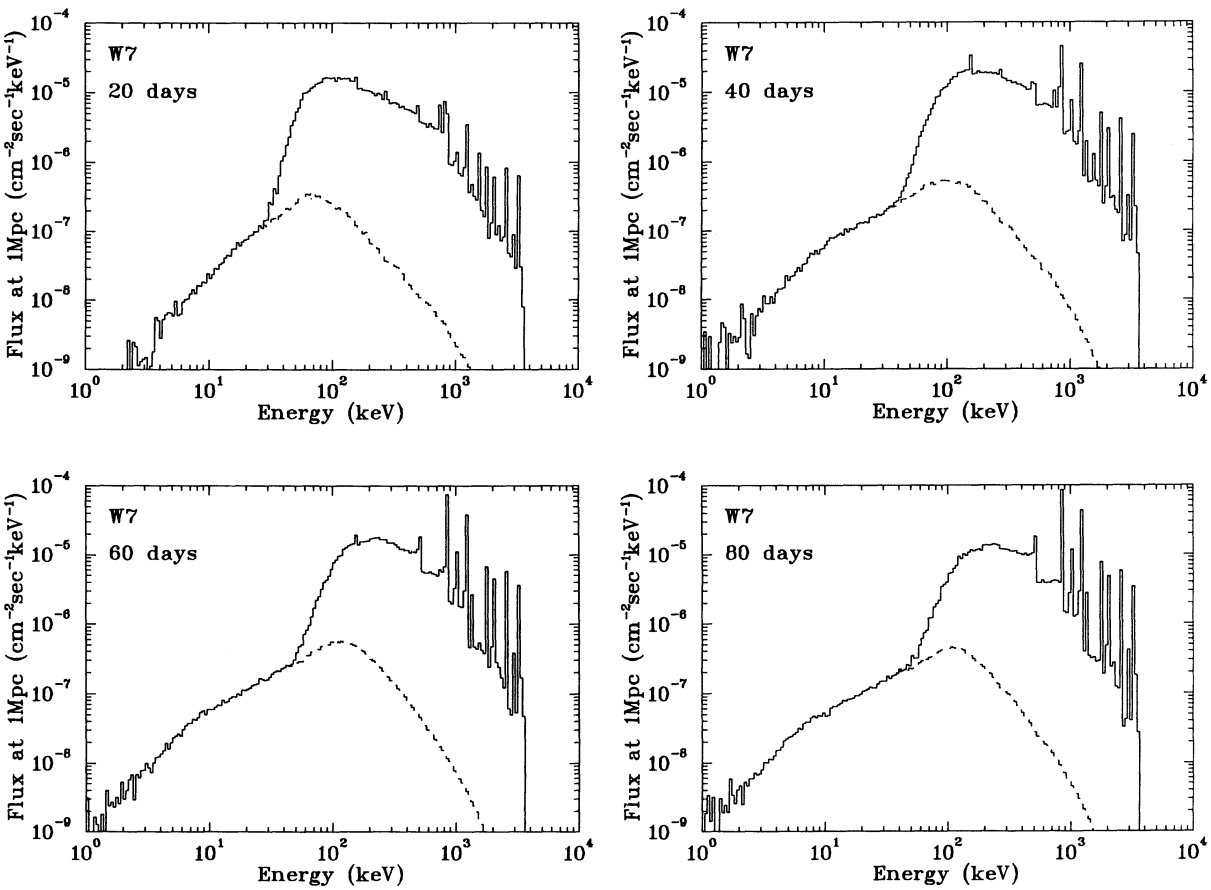

FIG. 13.—Total spectral flux from Type Ia model W7 at reference distance of 1 Mpc. Bremsstrahlung flux is very prominent below about 40 keV, roughly $F(\nu) \propto \nu^{1.5}$, depending on the age. Gamma lines are very strong (as in Burrows & The 1990), but the K shell X-ray fluxes are weak because of the opacity of the C and O cap on top of the nucleosynthesis products in W7. Compare with the fully mixed version in Fig. 14.

according to a $t = 20$ days calculation that we carried out to evaluate that question. The gamma continuum is so bright for Type Ia that it dominates the K shell vacancy rate for circumstellar Si (photoelectric + Compton). The bremsstrahlung are increasingly more important for lighter elements than Si. We will return below to a discussion of this ionization in Type Ib models for which the bremsstrahlung K vacancy rate is relatively more important.

One notices in Figure 13 that the K X-ray lines are very weak. This weakness is the result of photoelectric absorption in the overlying C and O cap on top of the heavy elements in W7; i.e., the cap in W7 is unmixed. Figure 14 confirms the K X-ray luminosity to be much stronger if the model assumes the heavy elements to be mixed to the surface. Model W7fm is a fully mixed version of model W7 (called W7e by Burrows & The 1990). The iron-group lines are especially strong, but intermediate-mass elements are also visible. The same mixing that increases the K X-rays decreases the bremsstrahlung continuum, however. The increased photoelectric opacity near the surface greatly obstructs the bremsstrahlung continuum, forcing it to emerge from shallower depths. The change of slope at 50 keV is less pronounced in the mixed model. It seems likely that Type Ia supernovae will indeed mix rapidly after the outburst, as discussed by Burrows and The. The results shown in Figure 14, for the same four times as in Figure 13, confirm Burrows and The's demonstration that the early line fluxes and continuum of gammas is much strengthened above 100 keV by this mixing. For the new emphasis taken in this work we repeat that the K X-rays are much strengthened by the mixing but that the bremsstrahlung continuum is *weakened*. The weakening of the bremsstrahlung is tabulated in the model summaries in Tables 3 and 4. They show $F^{\rm brem}$ to be weaker in each energy band for the mixed model W7fm. The mixing of Fe and Co and other heavy elements to the surface of W7fm has greatly increased its surface photoelectric opacity in these energy bands and the resultant weakening of the emerging continuum luminosity in those bands. The K shell vacancies leading to the K X-rays in Figure 14 are produced primarily by the Comptonized gammas. These K X-rays are much brighter in the mixed model because the K shell vacancies are now near the surface where the X-rays can be seen.

Other differences between W7 and W7fm can be seen in the comparison of Tables 3 and 4, and they merit understanding. The total recoil KE_C is smaller in the mixed W7fm because more of the gammas escape without scattering. The average recoil energy of a Compton event $\langle KE_C \rangle$ is also slightly lower in the mixed model. This is because the low-energy gammas, which are the ones that do not easily escape either model, still

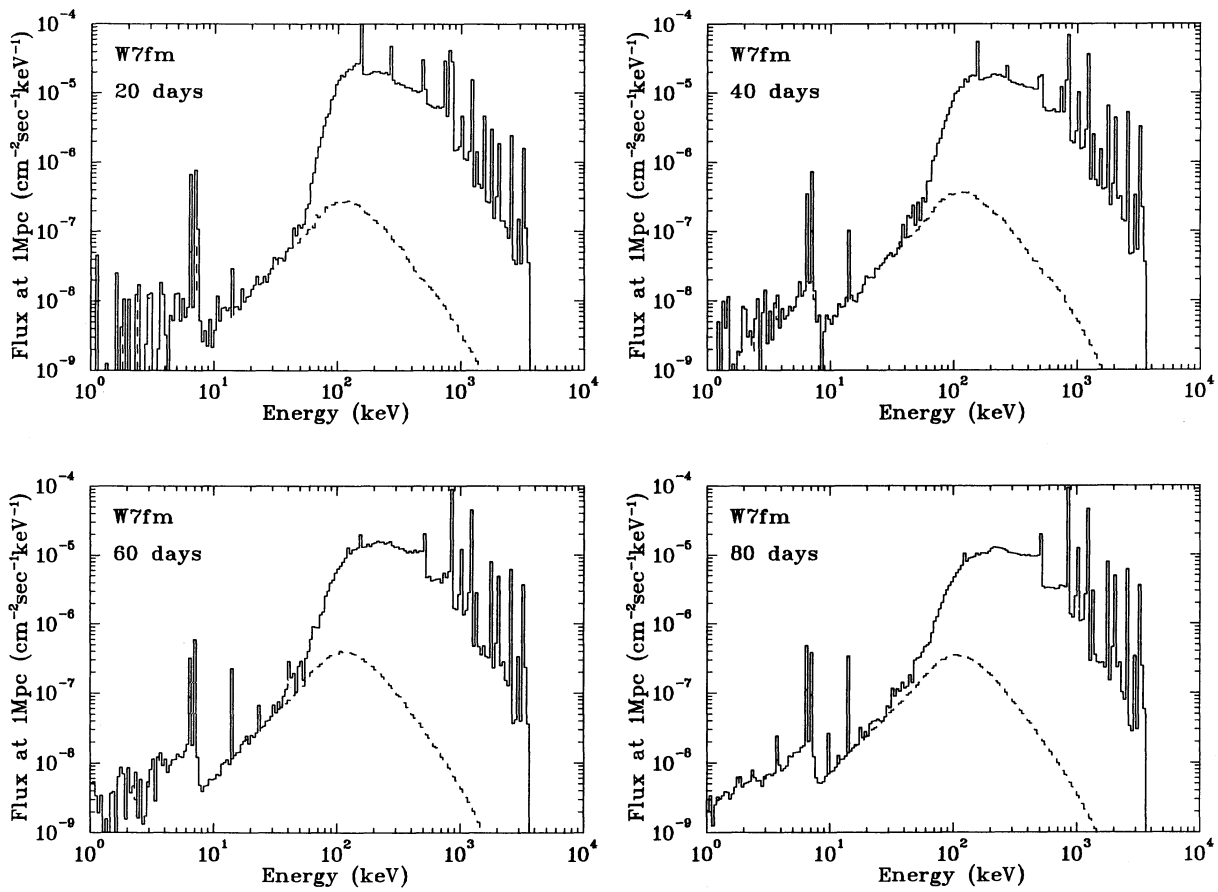

FIG. 14.—Fully mixed version of Type Ia model W7, to compare with the flux in the unmixed version (Fig. 13). Gamma lines and continuum above 1 MeV are little altered, but the bremsstrahlung luminosity is decreased by the larger photoelectric surface opacity from the admixed metals, the K X-rays are increased owing to the admixture of surface emitters, the photoelectric cutoff of the Comptonized tail moves to higher energy because of opacity increase, and the 14 keV ^{57}Co line becomes visible. In short the degree of mixing of Type Ia models is recorded by the bremsstrahlung below 50 keV and by the K X-rays. At late times the bremsstrahlung continuum is stronger below the Fe absorption edge near 7 keV than it is above it, again because of the opacity increase above 7 keV.

TABLE 4

MODEL W7fm CHARACTERISTICS

Time (days)	KE_C (ergs s^{-1})	$\overline{KE_C}$ (keV)	$Yield_{brem}$ (10^{-2})	E_{brem} (ergs s^{-1})	F^{brem} [a] (cm^{-2} s^{-1})	F^{brem}_{10-20} [a] (cm^{-2} s^{-1})	F^{brem}_{20-30} [a] (cm^{-2} s^{-1})	F^{brem}_{30-40} [a] (cm^{-2} s^{-1})	F^{brem}_{40-50} [a] (cm^{-2} s^{-1})	F^{brem}_{50-60} [a] (cm^{-2} s^{-1})
20.....	8.20×10^{42}	147	0.868	7.11×10^{40}	5.75×10^{-8}	9.05×10^{-8}	2.09×10^{-7}	3.98×10^{-7}	6.57×10^{-7}	9.29×10^{-7}
40.....	2.94×10^{42}	202	1.11	3.25×10^{40}	6.67×10^{-8}	1.13×10^{-7}	3.13×10^{-7}	5.49×10^{-7}	8.88×10^{-7}	1.25×10^{-6}
60.....	1.43×10^{42}	240	1.17	1.68×10^{40}	7.77×10^{-8}	1.39×10^{-7}	3.38×10^{-7}	6.14×10^{-7}	9.48×10^{-7}	1.38×10^{-6}
80.....	7.67×10^{41}	277	1.23	9.45×10^{39}	8.95×10^{-8}	1.48×10^{-7}	3.66×10^{-7}	6.44×10^{-7}	1.05×10^{-6}	1.54×10^{-6}

[a] Assuming distance of 1 Mpc and no interstellar absorption.

contribute their smaller contributions to $\langle KE_C \rangle$, whereas the high-energy ones having the largest recoil energies preferentially escape from the mixed model. The bremsstrahlung yield is smaller in the mixed model because of the reduction in the initial average kinetic energy of the recoils $\langle KE_C \rangle$. Figure 4 made it clear that higher electron energy increases the bremsstrahlung yield. So, of course, the total bremsstrahlung created within the model is for both reasons smaller for the mixed version W7fm.

10. He CORE EXPLOSION (TYPE Ib) SUPERNOVAE

We evaluate also a class of Type Ib supernova models evolving from Wolf-Rayet star progenitors leading to core-collapse explosions of their massive He cores (Ensman & Woosley 1988). They argued that the H-free spectrum and the rapid light curve could result if a massive star had lost its envelope in a prior wind. The gamma spectra themselves of such models have already been published by The, Clayton, & Burrows (1990b), who showed that this class of objects would be very bright, observable in the 847 keV line of ^{56}Co decay out to several Mpc by OSSE on *GRO*. They also showed that full mixing of those models would greatly reduce the Comptonized continuum near 50 keV by its increase of the photoelectric opacity in the outer mass zones. In this work we repeat those full spectra with emphasis on the new results—the bremsstrahlung luminosity and the photoinduced K X-rays from heavy elements.

Figure 15 repeats our previous (The et al. 1990b) calculation of the gamma spectrum of model WR6C at four distinct times, but also includes the very bright bremsstrahlung continuum. This continuum might eventually be observable, and it contains information distinct from that in the Compton contin-

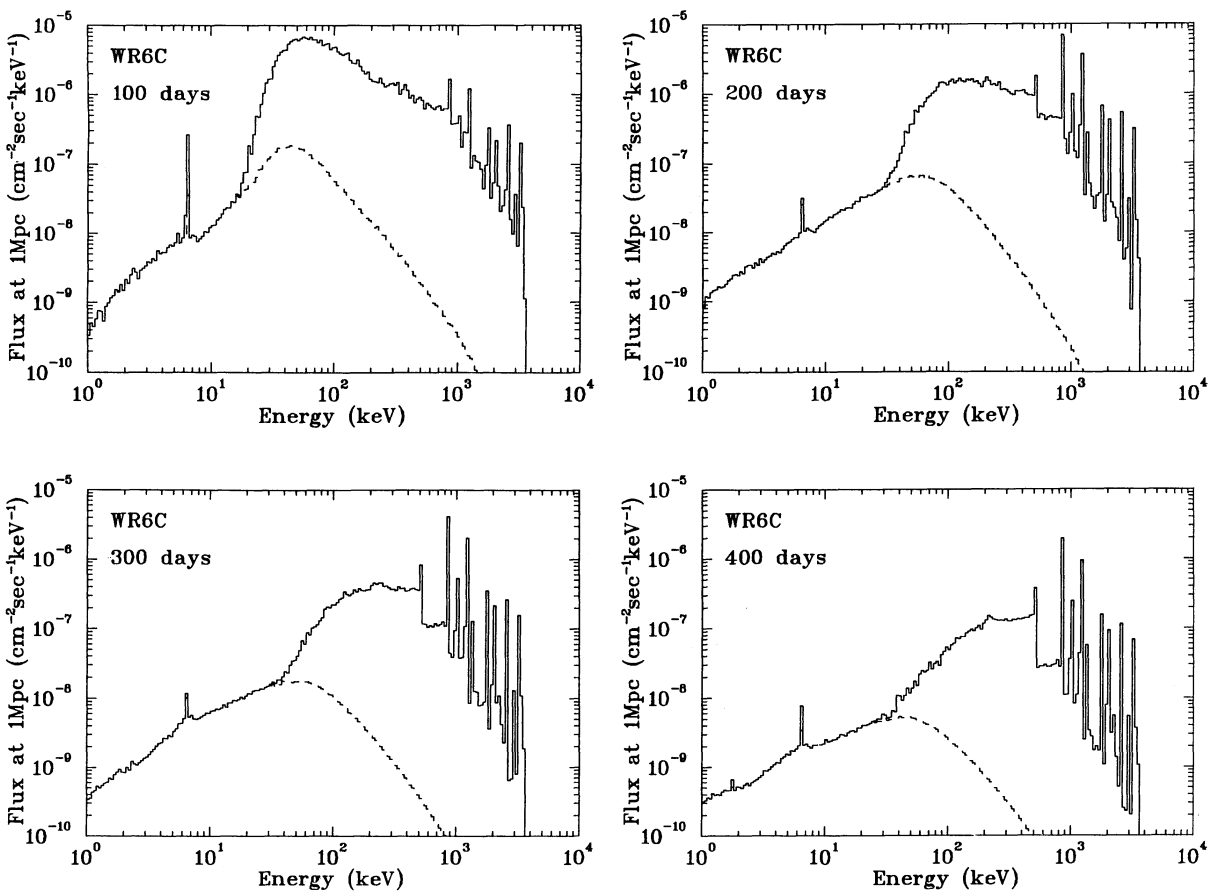

FIG. 15.—Flux at 1 Mpc reference distance of an exploding helium core model of a Type Ib supernova (Ensman & Woosley 1988). The bremsstrahlung luminosity of such objects is very bright in comparison with the Comptonized gammas. Fully mixed version is in Fig. 16.

uum. The ratio of bremsstrahlung to gamma continuum is higher for this object than for other supernova models that we have evaluated. This can be quantitatively expressed in terms of the K shell ionization rates of circumstellar atoms. Detailed consideration of circumstellar Si atoms around the 200 day luminosity, for example, shows that 25% of the Si K shell vacancies are due to bremsstrahlung and 75% to gammas (photoelectric + Compton scattering). Bremsstrahlung are increasingly more important for even lighter elements but less important for heavier ones. The $F(\nu) \propto \nu$ bremsstrahlung luminosity continues downward below 1 keV and therefore dominates the ionization of circumstellar He, for which such a spectrum produces tenfold more ionizations from the 0.1–1.0 keV range than it does above 1 keV. For comparison with a different supernova type, reference back to the 20 day spectrum of the Type Ia model W7 in Figure 13 shows by detailed integration that 12% of Si K vacancies result from bremsstrahlung. Thus we conclude that, especially for He, the bremsstrahlung ionization of circumstellar matter will be essential. Similar conclusions can be drawn concerning the origin of the emerging X-ray lines.

Figure 16 shows, as for Type Ia models, that not only the early gamma-line luminosity but also the X-ray–line luminosity is much increased by fully mixing the model. This comes about by placing more X-ray–line emitters (Si,... Fe,...) near the surface so that their radiations can emerge without photoelectric absorption. By tagging the ionization source of the emerging photons in our code we were able to show the relative importance of differing sources of photoionizations. Considering the 200 day panel of Figure 16, for instance, we find that bremsstrahlung produced slightly more than half of the observed photoinduced emerging K X-rays even for elements as heavy as Ca. The increased importance of bremsstrahlung within the interior itself for the K shell vacancy rate is easy to understand, because the emissivity curves (viz., Figs. 2 and 12) show that vastly more soft bremsstrahlung are created than ever emerge, but those bremsstrahlung are in large part absorbed in the creation of K shell vacancies. This comparison does not reflect, however, the even larger rate of K shell vacancies from collisions with the Compton-recoiling electrons themselves, as we evaluate and display in a subsequent work (The et al. 1991). The bremsstrahlung luminosity itself, however, is decreased by the mixing because the photoelectric opacity in the surface layers is increased. Although the measurement of the spectrum in the keV region remains a difficult problem for the future because of its faintness, we see from the comparisons of Figures 15 and 16 that it does contain clearer evidence of the mixing than does the high-energy spectrum. Table 5 and 6 summarized emission from these models.

11. CONCLUSION

This work has made much more explicit the intense radiation environment within a supernova whose light curve is powered by ^{56}Co radioactivity. Every process that depends upon that environment is impacted in some way by our results.

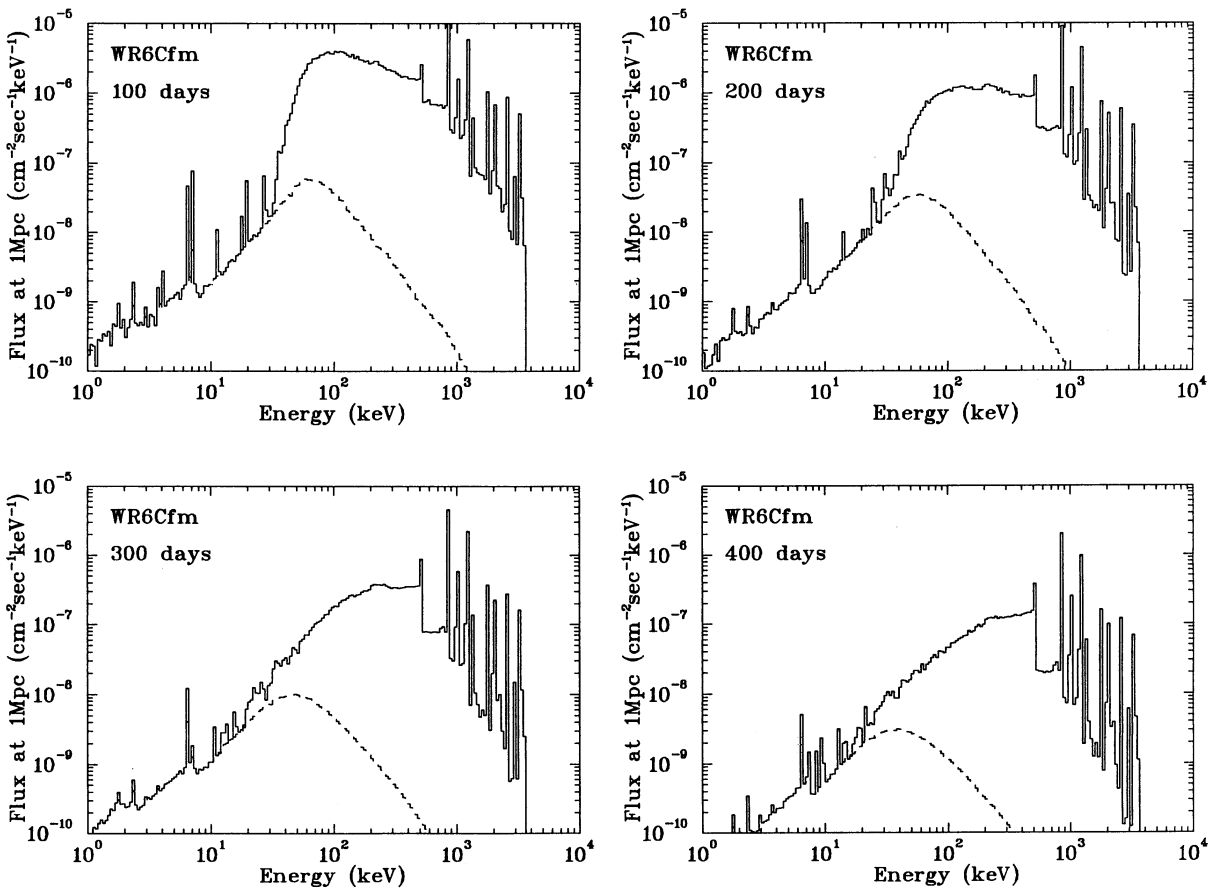

FIG. 16.—Flux from fully mixed version of WR6C, an exploding He core of a massive star advanced as a model of the Type Ib supernova. As in the case of Type Ia models, the mixing increases the K X-ray lines but lowers the X-ray continuum by virtue of increasing the photoelectric opacity.

TABLE 5

MODEL WR6C CHARACTERISTICS

Time (day)	KE_C (ergs s^{-1})	$\overline{KE_C}$ (keV)	$Yield_{brem}$ (10^{-3})	E_{brem} (ergs s^{-1})	$F^{brem\ a}_{1-10}$ ($cm^{-2}\ s^{-1}$)	$F^{brem\ a}_{10-20}$ ($cm^{-2}\ s^{-1}$)	$F^{brem\ a}_{20-30}$ ($cm^{-2}\ s^{-1}$)	$F^{brem\ a}_{30-40}$ ($cm^{-2}\ s^{-1}$)	$F^{brem\ a}_{40-50}$ ($cm^{-2}\ s^{-1}$)	$F^{brem\ a}_{50-60}$ ($cm^{-2}\ s^{-1}$)
100.....	6.95×10^{41}	145	5.70	3.96×10^{39}	6.06×10^{-8}	2.90×10^{-7}	8.35×10^{-7}	1.57×10^{-6}	1.79×10^{-6}	1.63×10^{-6}
200.....	9.03×10^{40}	266	6.09	5.49×10^{38}	7.04×10^{-8}	2.34×10^{-7}	3.73×10^{-7}	5.17×10^{-7}	6.33×10^{-7}	6.60×10^{-7}
300.....	1.61×10^{40}	355	6.27	1.01×10^{38}	3.20×10^{-8}	8.73×10^{-8}	1.31×10^{-7}	1.62×10^{-7}	1.73×10^{-7}	1.75×10^{-7}
400.....	3.63×10^{39}	399	6.17	2.24×10^{37}	1.33×10^{-8}	3.04×10^{-8}	4.42×10^{-8}	5.01×10^{-8}	5.28×10^{-8}	4.96×10^{-8}

[a] Assuming distance of 1 Mpc and no interstellar absorption.

TABLE 6

MODEL WR6Cfm CHARACTERISTICS

Time (days)	KE_C (ergs s^{-1})	$\overline{KE_C}$ (keV)	$Yield_{brem}$ (10^{-3})	E_{brem} (ergs s^{-1})	$F^{brem\ a}_{1-10}$ ($cm^{-2}\ s^{-1}$)	$F^{brem\ a}_{10-20}$ ($cm^{-2}\ s^{-1}$)	$F^{brem\ a}_{20-30}$ ($cm^{-2}\ s^{-1}$)	$F^{brem\ a}_{30-40}$ ($cm^{-2}\ s^{-1}$)	$F^{brem\ a}_{40-50}$ ($cm^{-2}\ s^{-1}$)	$F^{brem\ a}_{50-60}$ ($cm^{-2}\ s^{-1}$)
100.....	4.45×10^{41}	150	3.02	1.34×10^{39}	1.03×10^{-8}	4.14×10^{-8}	1.09×10^{-7}	2.22×10^{-7}	3.78×10^{-7}	5.37×10^{-7}
200.....	6.38×10^{41}	276	3.39	2.16×10^{38}	1.05×10^{-8}	4.52×10^{-8}	1.14×10^{-7}	2.08×10^{-7}	2.99×10^{-7}	3.40×10^{-7}
300.....	1.19×10^{40}	362	3.49	4.14×10^{37}	5.81×10^{-9}	2.40×10^{-8}	5.81×10^{-8}	8.62×10^{-8}	9.88×10^{-8}	9.53×10^{-8}
400.....	2.75×10^{39}	405	3.53	9.73×10^{36}	2.78×10^{-9}	1.15×10^{-8}	2.39×10^{-8}	3.00×10^{-8}	2.94×10^{-8}	2.56×10^{-8}

[a] Assuming distance of 1 Mpc and no interstellar absorption.

We have emphasized the Compton-recoil spectrum of the electrons and the bremsstrahlung that they create. It is tempting to call these "internal bremsstrahlung," despite the use of that term in beta-decay physics, because these photons are created within the supernova interior. This process seems to be the only one capable of a photon continuum below 20 keV from supernovae, because the photoelectric absorption is too severe a barrier to centrally produced photons. The only competitor, "external bremsstrahlung," arises from the circumstellar collision of the ejecta with surrounding matter. Our initial hope, therefore, was that the *Ginga* X-ray luminosities in 6–16 keV and 16–28 keV bands would arise naturally from this process. A secondary hope was that *ROSAT* would detect SN 1987A and that our calculations would provide an adequate explanation. Neither hope was fulfilled because of the weakness of the bremsstrahlung luminosity. The numbers of photons above 100 keV resulting from the Comptonized radioactivity-produced gammas generally exceed that produced by bremsstrahlung by at least 10^2–10^3, at least to external observers. As discouraging as that sounds, we have shown that the bremsstrahlung do nonetheless dominate the luminosity of supernovae between 1 and about 20 keV, except for a ^{57}Co nuclear line (Clayton 1974) at 14 keV and the Fe K X-ray at 6.4 keV (plus lighter elements having weaker lines). The number spectrum of the X-ray flux is approximately $F(\nu) \propto \nu^{1.0-1.5}$, depending on the model. That bremsstrahlung dominance continues downward in energy toward the ultraviolet, because the suprathermal component of the electron gas is the major source of suprathermal photoluminosity at photon energies in excess of those that can be provided by radiative recombination. Our calculations of the emergent bremsstrahlung constitute only a low limit to the expectations, because electrons in the envelope actually move toward the surface as they slow down, and they also radiate preferentially in the forward direction rather than isotropically, and because clumping and ionization may lower the photoelectric opacity from the value assumed by us for our calculations.

We have shown for several classes of supernova model that evidence of mixing can be obtained at late times from the 1–20 keV spectrum. This contrasts with the gammas, for which mixing has a strong effect only at early times. The fully mixed versions of all types show (1) stronger K X-rays from heavy elements, (2) weaker bremsstrahlung continuum, and (3) discontinuity in the size of bremsstrahlung continuum near the 7 keV K edge of Fe, above which the continuum continues with the same slope but lower amplitude. Our figures display these late time differences markedly for W7 and WR6C. Despite the technical difficulty in observing this weak energy range, the late-time diagnostic capability that we have displayed may ultimately be of high importance to the diagnosis of supernova structure.

Direct detectability aside, the indirect effects on the ionization balance, both within and without the supernova, must be evaluated for the specific supernova model in question. We have attempted to facilitate this by showing that the bremsstrahlung emissivity is about 1% of the Compton-recoil power for Type Ia and about 0.3% for Type II, and that in both cases that emissivity follows a $E^{-1.3}$ power law. By propagating these photons we have shown the surface transmission rate to increase roughly linearly with frequency—slightly steeper for some models. We have also presented for the first time the explicit spectrum of electron recoils from the Compton events and have shown that they can be matched by a predictable spectrum $(1 + E/E_0)^{-n}$, where $n = 2.0$ for Type II and $n = 2.5$ for Type Ia and where $E_0 = 18$ keV for Type II and 150 keV for Type Ia (approximately). We have also presented a careful exposition of the physics of bremsstrahlung emissivity and of the yields of stopping electrons of differing initial energies in differing compositions. More exact evaluations will require calculation of each explicit supernova model. Still to come are our evaluations of the abundant ionization events by collisions during the stopping of the recoil electrons (The, et al. 1991) and of certain photon tags that we have introduced (e.g., the number of collisions producing the Compton continuum, etc.). We submit this work as one additional step in the elucidation of the violent interiors of supernovae.

This research was supported by Naval Research Laboratory

grant N00014-89-J-2034 under the NASA contract for the OSSE Spectrometer DPRS-10987 on the *Gamma-Ray Observatory*. We thank Stan Woosley for the detailed listing of his models 10hmm and WR6C, and Ken Nomoto for his listings of SN 11E1 and W7. We profited from several conversations with Adam Burrows.

REFERENCES

Burrows, A., & The, L.-S. 1990, ApJ, 360, 626
Clayton, D. D. 1974, ApJ, 188, 155
Clayton, D. D., Colgate, S. A., & Fishman, G. J. 1969, ApJ, 155, 75
Clayton, D. D., & Woosley, S. E. 1969, ApJ, 157, 1381
Cook, W. R., Palmer, D. M., Prince, T. A., Schindler, S., Starr, C. H., & Stone, E. C. 1988, ApJ, 334, L87
Ensman, L. M., & Woosley, S. E. 1988, ApJ, 333, 754
Graham, J. R. 1988, ApJ, 335, L53
ICRU Report 37. 1984, Stopping Powers for Electrons and Positrons (Bethesda: Int. Commission on Radiation Units and Measurements)
Jauch, J. M., & Rohrlich, F. 1976, The Theory of Photons and Electrons, 2d ed. (New York: Springer), 364
Johnson, W. N., et al. 1989, in Gamma Ray Observatory Science Workshop, ed. W. N. Johnson (Washington: GPO), 2
Kumagai, S., Shigeyama, T., Nomoto, K., Itoh, M., Hishimura, J., & Tsuruta, S. 1989, ApJ, 345, 412
Lee, C. M., Kissel, L., & Pratt, R. H. 1976, Phys. Rev. A, 13, 1714
Leising, M. D., & Share, G. H. 1990, ApJ, 357, 638
Lepp, S., Dalgarno, A., & McCray, R. 1990, ApJ, 358, 262
Mahoney, W. A., Varnell, L. S., Jacobsen, A. S., Ling, J. C., Radocinski, R. G., & Wheaton, W. M. 1988, ApJ, 334, L81
Masai, K., Hayakawa, S., Inoue, H., Itoh, H., & Nomoto, K. 1988, Nature, 335, 804
Matz, S. M., Share, G. H., Leising, M. D., Chupp, E. L., Vestrand, W. T., Purcell, W. R., Strickman, M. S., & Reppin, C. 1988, Nature, 331, 416
Nomoto, K., Shigeyama, T., Kumagai, S., & Hashimoto, M. 1988, Proc. Astr. Soc. Australia, 7, 490
Nomoto, K., Thielemann, F.-K., & Yokoi, K. 1984, ApJ, 286, 664
Pinto, P. A., & Woosley, S. E. 1988a, ApJ, 329, 820
———. 1988b, Nature, 333, 534
Pratt, R. H., & Tseng, H. K. 1975, Phys. Rev. A, 11, 1797
Pratt, R. H., Tseng, H. K., Lee, C. M., Kissel, L., MacCallum, C., & Riley, M. 1977, Atomic Data and Nucl. Data Tables, 20, 175
Rester, A. C., Eichhorn, G., Coldwell, R. L., Trombka, J. I., Starr, R., & Lasche, G. P. 1989, ApJ, 342, L71
Rohrlich, F., & Carlson, B. C. 1953, Phys. Rev., 93, 38
Sandie, W. G., Nakano, G. H., Chase, L. F., Fishman, G. J., Meegan, C. A., Wilson, R. B., Paciesas, W. S., & Lasche, G. P. 1988, ApJ, 334, L91
Spicer, D. S., Clark, R. W., & Maran, S. P. 1990, ApJ, 356, 549
Tanaka, Y. 1988, in IAU Coll. 108, Atmospheric Diagnostics of Stellar Evolution, ed. K. Nomoto, Lecture Notes in Physics, 305, 399
The, L.-S., Bridgman, W. T., & Clayton, D. D. 1991, in preparation
The, L.-S., Burrows, A., & Bussard, R. 1990a, ApJ, 352, 731
The L.-S., Clayton, D. D., & Burrows, A. 1990b, in IAU Symp. 143, Wolf-Rayet Stars in Galaxies, ed. K. A. van der Hucht & B. Hidayat (Dordrecht: Kluwer), 537
Tueller, J., Barthelmy, S., Gehrels, N., Teegarden, B. J., Leventhal, M., & MacCallum, C. J. 1990, ApJ, 351, L41
Woosley, S. E., Pinto, P. A., & Hartmann, D. H. 1989, ApJ, 346, 395
Xu, Y., Sutherland, P., McCray, R., & Ross, R. R. 1988, ApJ, 327, 197